nature cell biology

TECHNICAL REPORT

https://doi.org/10.1038/s41556-018-0147-7

Self-assembly of embryonic and two extra-embryonic stem cell types into gastrulating embryo-like structures

Berna Sozen[1,2,10], Gianluca Amadei[1,10], Andy Cox[1], Ran Wang[3], Ellen Na[4], Sylwia Czukiewska[1], Lia Chappell[5], Thierry Voet[5,6], Geert Michel[7], Naihe Jing[3,8], David M. Glover[9] and Magdalena Zernicka-Goetz[1*]

Embryonic stem cells can be incorporated into the developing embryo and its germ line, but, when cultured alone, their ability to generate embryonic structures is restricted. They can interact with trophoblast stem cells to generate structures that break symmetry and specify mesoderm, but their development is limited as the epithelial–mesenchymal transition of gastrulation cannot occur. Here, we describe a system that allows assembly of mouse embryonic, trophoblast and extra-embryonic endoderm stem cells into structures that acquire the embryo's architecture with all distinct embryonic and extra-embryonic compartments. Strikingly, such embryo-like structures develop to undertake the epithelial–mesenchymal transition, leading to mesoderm and then definitive endoderm specification. Spatial transcriptomic analyses demonstrate that these morphological transformations are underpinned by gene expression patterns characteristic of gastrulating embryos. This demonstrates the remarkable ability of three stem cell types to self-assemble in vitro into gastrulating embryo-like structures undertaking spatio-temporal events of the gastrulating mammalian embryo.

The mammalian embryo is built from three distinct tissues: the embryonic tissue or epiblast, which generates the body of the embryo, and two extra-embryonic tissues—the trophectoderm, which generates the placenta, and the primitive endoderm, which generates the yolk sac. As the embryo implants, it undergoes a morphological transformation during which primitive endoderm-derived visceral endoderm (VE) triggers remodelling of the epiblast into a polarized cellular rosette that evolves to undertake lumenogenesis[1,2]. This is followed by cavitation of the adjacent trophectoderm-derived extra-embryonic ectoderm (ExE) and finally the fusion of these cavities to form the single pro-amniotic cavity[3]. The signalling interactions between these tissues are important for the embryo to break its symmetry to establish anterior and posterior identity and initiate gastulation[4,5].

Embryonic stem (ES) cells can be incorporated into the developing embryo and its germ line[6,7]. However, when cultured alone, their ability to mimic embryogenesis is restricted[8–10], and the resulting structures neither acquire embryo architecture nor correctly recapitulate gastrulation. To address this, we previously allowed ES cells to cooperate with trophoblast stem (TS)[11] cells in vitro in a three-dimensional extracellular-matrix scaffold[3]. This led them to form embryo-like structures that resemble early post-implantation embryos with an ES-derived embryonic compartment and a TS-derived extra-embryonic compartment. These structures develop further and break symmetry to undertake the specification of nascent mesoderm and primordial germ cells (PGCs) at the posterior[3]. However, establishment of the anterior and the key morphogenetic events of gastrulation, namely the epithelial–mesenchymal transition (EMT), were limited in this system. We hypothesized that this was because crosstalk between all three tissues would be required to properly recapitulate embryogenesis in vitro, and these structures were missing the third tissue, the primitive endoderm-derived VE.

Indeed, the VE is known to play important roles during embryogenesis. First, it develops to surround both embryonic and extra-embryonic compartments and then becomes regionalized and develops a signalling centre that will enhance development of the anterior–posterior axis by repressing Nodal and Wnt signalling on the future anterior[12,13]. Second, it provides a barrier for migration of embryonic cells undertaking the EMT during gastrulation to form mesoderm. Finally, migrating embryonic cells progressively displace VE cells to generate the definitive endoderm[14,15].

Here, we wished to test the hypothesis that crosstalk between all three stem cell types found in the natural embryo would enable the generation of whole embryo-like structures able to exhibit the cell rearrangements of gastrulation. To achieve this, we established culture conditions allowing the stem cell lines for all three tissues that comprise mouse embryo—ES, TS and extra-embryonic-endoderm (XEN)[16] cells—to cooperate in vitro. We show that this cooperation results in the spontaneous self-assembly of structures that are remarkably similar to natural mouse embryos and contain all three embryonic and extra-embryonic compartments. We show that these

[1]Mammalian Embryo and Stem Cell Group, Department of Physiology, Development and Neuroscience, University of Cambridge, Cambridge, UK. [2]Department of Histology and Embryology, Faculty of Medicine, Akdeniz University, Antalya, Turkey. [3]State Key Laboratory of Cell Biology, CAS Center for Excellence in Molecular Cell Science, Shanghai Institute of Biochemistry and Cell Biology, Chinese Academy of Sciences, Shanghai, China. [4]Department of Cardiology, Charité, Berlin, Germany. [5]Wellcome Sanger Institute, Wellcome Genome Campus, Cambridge, UK. [6]Laboratory of Reproductive Genomics, Department of Human Genetics, KU Leuven, Leuven, Belgium. [7]Transgene Technologies, Charité, Berlin, Germany. [8]School of Life Science and Technology, ShanghaiTech University, Shanghai, China. [9]Department of Genetics, University of Cambridge, Cambridge, UK. [10]These authors contributed equally: Berna Sozen, Gianluca Amadei. *e-mail: mz205@cam.ac.uk

embryo-like structures develop to undertake anterior–posterior patterning and morphogenesis, leading to the key spatio-temporal events of gastrulation, including the EMT and the specification of mesoderm and definitive endoderm.

Results

Establishing conditions for spontaneous assembly of ES, TS and XEN cells into embryo-like structures. To address the hypothesis that crosstalk between the three stem cell types in vitro would permit generation of embryo-like structures with all three compartments, as is the case in natural embryos, we seeded single-cell suspensions of ES, TS and XEN cells in medium supporting the proliferation of all these cell types into inverted-pyramidal microwell plates, allowing cells to aggregate (see Methods). At the optimized cell density, the three cell types spontaneously underwent self-organization into multicellular aggregates within 24 h. After 96 h, approximately 70% of multicellular aggregates contained all three cell types. Of these, 29.8% ($n = 130/435$) had single adjoining ES-derived embryonic and TS-derived extra-embryonic compartments surrounded by a layer of XEN cells, and were strikingly similar in morphology to mouse embryos at 5–6 days after fertilization (Fig. 1a–c, Supplementary Fig.1a,b and Supplementary Movie 1). In agreement with their morphology, these structures expressed markers characteristic of the three tissues of the embryo (Fig. 1d,e). Cell numbers in the ES-, TS- and XEN-derived compartments after 96 h of culture were similar to those in the embryonic and extra-embryonic compartments of embryos cultured in vitro until 5.5 day after fertilization (Fig. 1f). We named these spontaneously organized embryo-like structures, ETX (ES + TS + XEN) embryos.

Mesoderm and primordial germ-cell-like cell specification. We first examined the development of ETX embryos to assess to what extent it was similar and different from the development of natural embryos and of the previous synthetic embryos (ET embryos) we had generated from only ES and TS cells[3]. Several developmental events followed similar spatio-temporal patterns. This included asymmetric expression of the mesoderm marker, *T/Brachyury*, in the ES compartment close to the TS compartment boundary 4.25 days after plating and extending towards the distal tip by day 5.5, thus resembling *T/Brachyury* expression in early (E6.5) to mid-streak (E7.0) stage embryos (Supplementary Fig. 2a,b; 42% ETX embryos, $n = 101$; 90% E6.5 embryos, $n = 20$). The ratio of *T/Brachyury*-expressing to total cells in the ES compartment of these ETX embryos was significantly higher than in synthetic embryos generated from only ES and TS cells and similar to embryos at equivalent developmental stage (Supplementary Fig. 2c,d). In contrast, the majority of structures formed from ES and XEN cells alone did not express *T/Brachyury* in these conditions, indicating that this is promoted by signalling from the TS-derived compartment (Supplementary Fig. 2e–g).

In natural embryogenesis, primordial germ-cell-like cells (PGCs) are specified at the posterior. To address whether this is also the case for ETX embryos, we next built them using ES cells expressing a *T*:GFP reporter. We found that expression of PGC markers (assessed on protein and mRNA levels) was induced at day 6 at the boundary between the ES- and TS-derived compartments and proximal to the mesodermal domain (Supplementary Fig. 2h–i). We also found an inverse gradient of Oct4 and *T/Brachyury* protein across the ES-derived-embryonic compartment at this stage (Supplementary Fig. 2j), indicating that not only the posterior, but also aspects of the anterior pattern became established as development of ETX embryos progressed, reminiscent of natural embryogenesis. These results indicate that ETX embryos develop to break symmetry close to the ES/TS compartment boundary to induce expression of mesoderm and PGC markers.

XEN cell layer, basal membrane and cavity development. Lumenogenesis of embryos requires signalling from the basement membrane generated by the VE[1]. We therefore asked whether this requirement could be met by the XEN layer in ETX embryos. We found that the XEN layer formed a laminin-containing basement membrane where the XEN cells met the ES- and TS-derived compartments (Supplementary Fig. 3a). The localization of E-cadherin and podocalaxin indicated that this basal membrane was functional, because it induced polarization and lumenogenesis in ES- and TS-derived compartments (Supplementary Fig. 3b–d), and basement membrane was not detectable between these compartments at day 5 (Supplementary Fig. 3e,f). Thus, by providing components of the basal membrane to enable ES and TS cell maturation, the XEN layer appears to fulfil one role of the VE.

Regionalization of the XEN cell layer. During embryogenesis, VE undergoes functional regionalization. The VE overlying the embryonic compartment develops as a heterogeneous mix of squamous and cuboidal cells at E5.25, which resolves at E6.75 into defined squamous VE. In contrast, the VE overlying the ExE develops predominantly cuboidal morphology. We found that as ETX embryos developed, XEN cells overlying the ES-derived compartment became squamous by day 5, whereas those overlying the TS-derived compartment remained cuboidal (Fig. 2a), thus resembling VE compartmentalization in natural embryos (Fig. 2b). The proportions of cells between the embryonic and extra-embryonic XEN layers in ETX embryos were similar to the distribution in the VE of natural embryos (Fig. 2c). Thus, cellular morphogenesis of the ETX embryo XEN layer resembles natural VE.

Further regionalization of VE leads to the formation of anterior visceral endoderm (AVE), which secretes Lefty1, DKK1 and Cerl to antagonize posteriorizing morphogens and establish an anterior–posterior gradient of Nodal within the epiblast[17]. To assess Nodal patterning as the ETX embryos developed, we built them using ES cells expressing the Nodal 'highly bound element' HBE-YFP reporter[18]. At 4 days, the ETX embryos showed uniform Nodal expression throughout the ES-derived compartment (Fig. 3a and Supplementary Fig. 4a–c; 90%, $n = 18/20$), becoming asymmetric and higher on the presumptive posterior side at day 5 (Fig. 3b and Supplementary Fig. 4a–c; 80%, $n = 16/20$).

To assess whether this could be a response to antagonism by a developing AVE-like domain, we assessed the expression of Lefty1[17] at days 4 and 5. We found that some ETX embryos showed asymmetric Lefty1 expression in the XEN layer (Fig. 3c, $n = 7/17$), indicative of AVE-like specification. On days 4 to 5, increased Lefty1 immunofluorescence became evident on the side of the XEN layer opposite *T/Brachyury* or Nodal HBE-YFP expression (Fig. 3c–e). Similar regionalization of gene expression was further assessed by in situ hybridization to localize *Cerl*, *Nodal*, *T/Brachyury*, *Cripto*, *Wnt3* and *Bmp4* in day 4 and 5 ETX embryos in comparison to natural embryos (Supplementary Fig. 4d).

We next examined the localization of Otx2, which also regulates AVE and the anterior–posterior axis specification[19]. We found Otx2 was expressed only in XEN cells overlying the embryonic, and not the extra-embryonic compartment (Fig. 3f, 42% $n = 20$) and became progressively restricted to one side of ETX embryos from day 4 to 5, resembling Otx2 expression in E5.75–E6.75 embryos (Fig. 3f). Together, these results indicate that the XEN layer in the ETX embryo undergoes regionalization and, at least in some structures, can develop to express AVE markers on the side opposite posterior *T/Brachyury* and Nodal expression, thus mimicking AVE specification and localization.

Cell migratory events characteristic of the EMT at gastrulation. During embryogenesis, epiblast cells expressing *T/Brachyury* undertake the EMT and ingress into the space between the epiblast

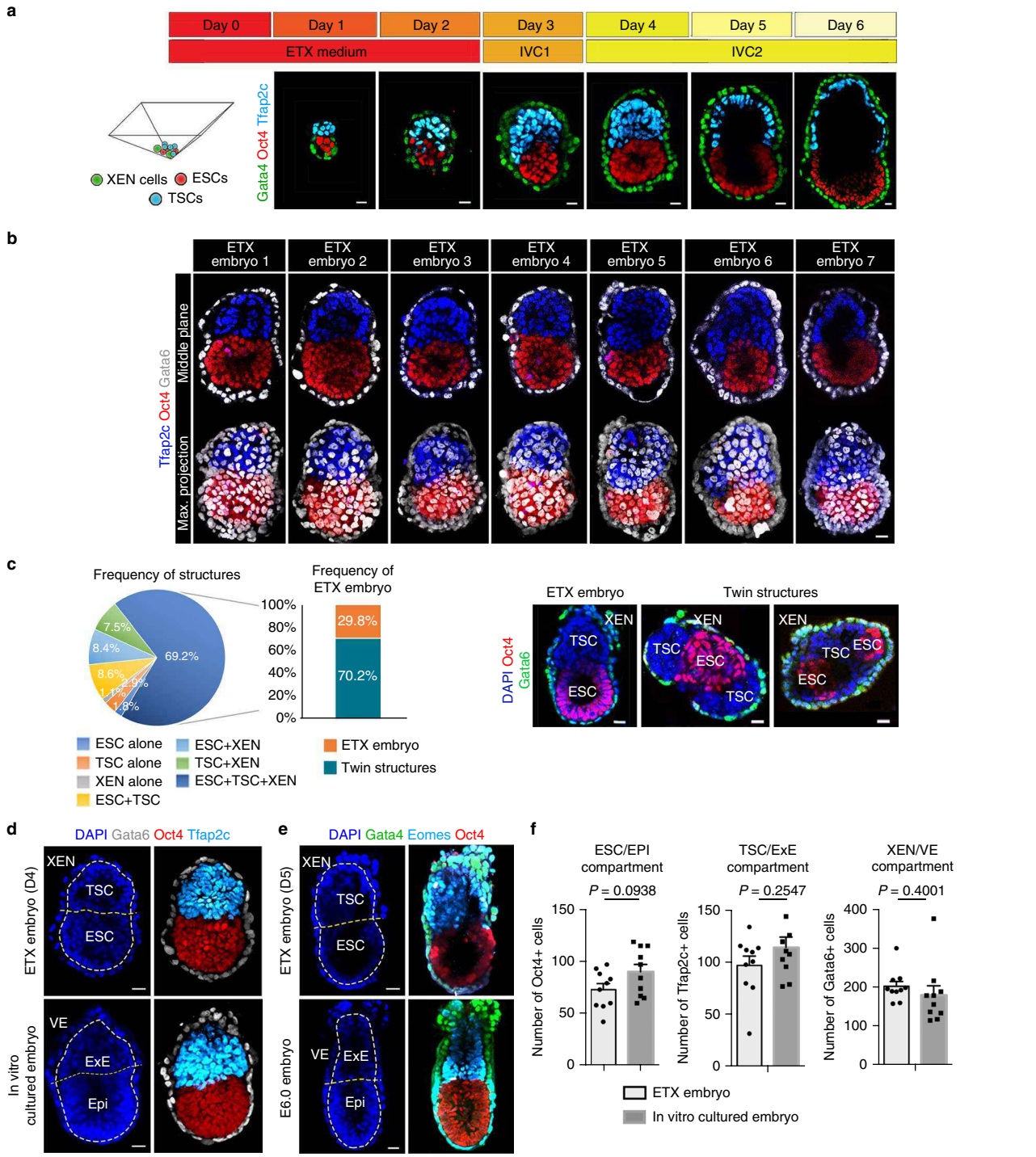

Fig. 1 | Self-assembly of embryo-like structures, ETX embryos. a, Schematic of an AggreWell with ES, TS and XEN cells on day 0, and representative examples of ETX embryos stained for lineage markers after progressive times in culture. Ten experiments. Scale bar, 20 μm. **b**, Representative examples of ETX embryos generated from a typical experiment after 4 days demonstrate three distinct compartments. Lineage markers: Oct4, red (embryonic); Tfap2c, blue, and Gata6, grey (extra-embryonic). Ten experiments. Scale bar, 20 μm. **c**, Frequency of structures comprising three stem cell types (ES, TS and XEN) compared to other combinations of stem cell types. A total of 435 structures were scored from three separate experiments. Pie chart: After 4 days, 69.2% of structures comprised three lineages; 24.7%, two lineages; and rarely a single cell type (1.87%, ES; 2.9%, TS; 1.1%, XEN). Bar chart: Of structures with three lineages, 29.8% were cylindrical with single adjoining ES and TS cell compartments surrounded by a XEN layer corresponding to ETX embryos (leftmost image); the remaining twin structures had either two TS (middle image) or ES (rightmost image) compartments at polar positions. ESC, embryonic stem cell; TSC, trophoblast stem cell; XEN, extra-embryonic endoderm stem cells. **d**,**e**, Immunostaining of ETX embryos after 4 days (**d**, top, 15 embryos) or 5 days (**e**, top, 10 embryos) of culture compared to natural embryo cultured for 48 h from blastocyst stage, equivalent to E5.5 (**d**, bottom, 10 embryos) or E6.0 embryo (**e**, bottom, 8 embryos) collected in three experiments. Yellow dashed line outlines embryonic/extra-embryonic border; white dashed line demarcates VE/XEN layer. Non-nuclear, unspecific anti-Oct4 VE fluorescence was removed from E6.0 embryo to enable visualization of the Gata4-positive VE cells. Scale bars, 20 μm. **f**, Quantification of mean embryonic and extra-embryonic cells in day 4 ETX embryos and cultured embryos equivalent to E5.5. EPI, epiblast. Two-sided Student's *t*-test, $n = 10$ ETX embryos per group, three experiments, not significant. Columns are means ± s.e.m.

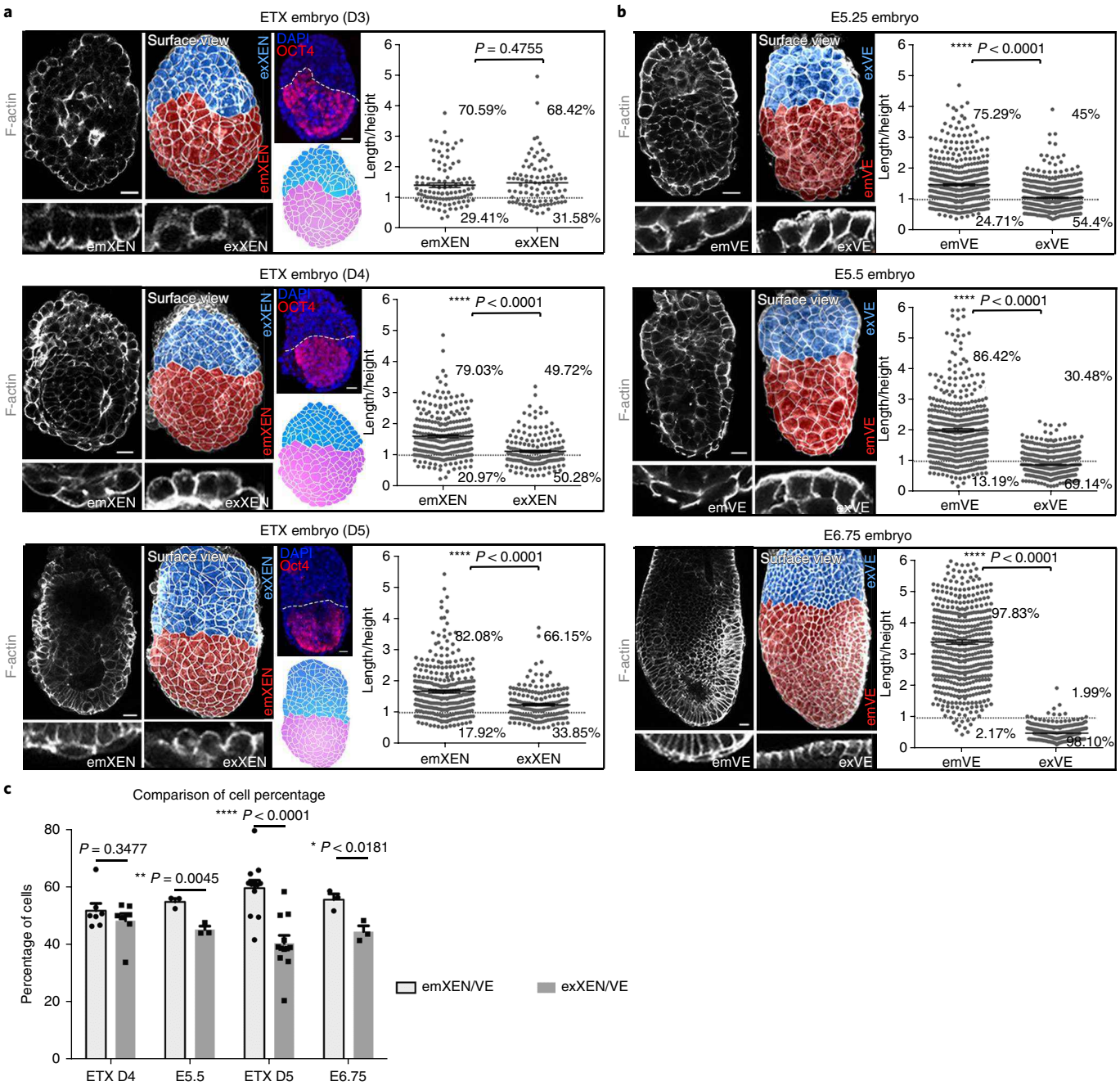

Fig. 2 | XEN cell layer in embryo-like structures. a, ETX embryos after 3 (D3, 9 embryos), 4 (D4, 8 embryos) and 5 (D5, 17 embryos) days of culture stained for F-actin to reveal the shape of XEN cells. Middle image, Surface rendering of ETX embryo showing the embryonic (em) compartment (red) and the extra-embryonic (ex) compartment (blue). Top right image, Boundary (dashed lines) of em and exXEN layer based on the boundary of Oct4 immunofluorescence. Bottom right image, Tracing of em and exXEN layer of ETX embryos based on F-actin immunofluorescence. Bottom images, Magnified fields showing em (left) or ex (right) XEN cells to highlight cell shape. Scatter plots show cell aspect ratios in the XEN layer. The mean cell aspect ratio is significantly different between ex- and emXEN compartments of ETX embryos at days 4 and 5. Each dot represents a cell. Values less than 1 indicate cells with predominant cuboidal morphology; values greater than 1 indicate cells with prevalent squamous morphology. Two-sided Student's *t*-test with Welch's correction. Day 3, $n = 102$ emXEN cells, $n = 95$ exXEN cells; day 4, $n = 267$ emXEN cells, $n = 181$ exXEN cells; day 5, $n = 318$ emXEN cells, $n = 191$ exXEN cells. Plots show means ± s.e.m. (black lines). Scale bars, 20 µm. **b**. Natural embryos at E5.25 (14 embryos), E5.5 (16 embryos) and E6.75 (5 embryos) stained for F-actin to reveal cell shape in the VE layer. Right image, Surface rendering of embryo showing embryonic (em) compartment (red), extra-embryonic (exe) compartment (blue). Bottom images, Magnified fields showing em (left) or ex (right) VE cells to highlight the cell shape. Scatter plots show cell aspect ratios in VE overlying ex and em compartments with time. Each dot represents a cell. Value less than 1 indicate cuboidal cells; value greater than 1 indicate squamous cells. Two-sided Student's *t*-test with Welch's correction. E5.25, $n = 509$ emVE cells, $n = 500$ exVE cells; E5.5, $n = 508$ emVE cells, $n = 538$ exVE cells; E6.75, $n = 505$ emVE cells, $n = 502$ exVE cells. Plots show means ± s.e.m. (black lines). Scale bars, 20 µm. **c**, Comparison of proportions of cells in em- and exXEN layer in ETX embryos ($n = 7$ day 4, $n = 12$ day 5 ETX embryos) versus VE layer of natural embryos ($n = 3$ E5.5, $n = 3$ E6.75 embryos). Two-sided Student's *t*-test. Columns are means ± s.e.m.

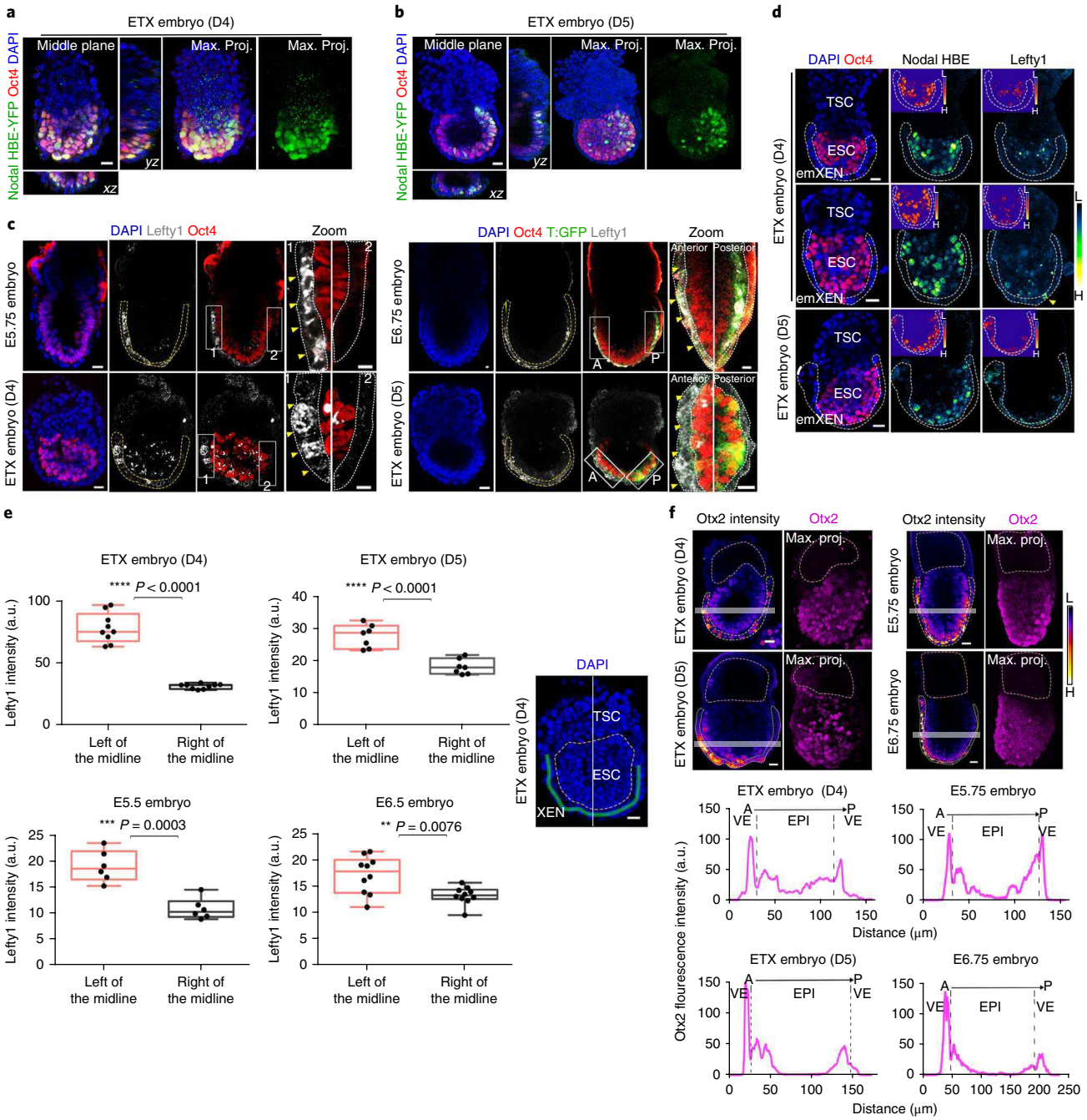

Fig. 3 | Regionalization within the XEN cell layer in ETX embryos. a,**b**, Representative ETX embryos built from Nodal HBE-YFP ES cells cultured for 4 or 5 days. Orthogonal *xz* and *yz* views are shown. 20 ETX embryos per group, three experiments. Scale bars, 20 μm. **c**. Lefty1 immunostaining of E5.75 (top left) and E6.75 (top right) natural embryos, and day 4 (bottom left) and day 5 (bottom right) ETX embryos. Yellow dashed line demarcates the embryonic VE/XEN layer; white boxes, magnified region; yellow arrowheads, Lefty1 positive VE/XEN cells; white dashed lines outline the border of the VE or XEN layer. Epiblast or ES compartment occasionally displayed low Lefty1 expression. Non-nuclear anti-Oct4 staining of VE represents non-specific binding. 7/7 natural embryos; 7/17 ETX embryos with asymmetric Lefty1, three experiments. A, anterior; P, posterior. Scale bars, 20 μm. Scale bars in zoomed images, 10 μm. **d**, Representative ETX embryos generated from Nodal HBE-YFP ES cells with uniform Nodal expression in the ES compartment and no Lefty1 expression (top) or induced Lefty1 expression in the XEN layer (arrowhead, middle) and Nodal gradient in the ES compartment with Lefty1 expression on the opposite side of the XEN layer (bottom). Nodal HBE-YFP and Lefty1 signal pseudocoloured with 'fire' lookup table in Fiji to highlight intensity gradients. White dashed line demarcates the embryonic VE/XEN layer. Boxed insets show embryonic compartment as a gradient map. L, low; H, high. 15 ETX embryos, three experiments. **e**, Quantification of asymmetric Lefty1 immunofluorescence intensity in the XEN or VE layer in representative embryos shown in **c**. Representative image of an ETX embryo (right) indicates line of intensity profiles along the XEN layer. White line indicates the midline of the structure; dashed lines outline the ES-derived compartment. Box plots represent $n = 9$ *z* planes for day 4, $n = 7$ *z* planes for day 5 ETX embryos; $n = 6$ *z* planes for E5.5, $n = 10$ *z* planes for E6.75 embryos (see Methods). Two-sided Student's *t*-test. Box plots show means ± s.e.m. Scale bar, 20 μm. **f**, 42.5% (12/28) of ETX embryos displayed Otx2 induction in the emXEN region. The 'Fire' pseudocolour lookup table in Fiji was used to highlight intensity gradients. L, low; H, high. Yellow dashed lines outline the emXEN/VE region. White lines indicate the plane used to plot intensity profiles (below). Purple dashed lines outline TS cell-derived extra-embryonic compartment or ExE for clarity. Scale bar, 20 μm; 20 ETX embryos, five experiments; 10 natural embryos, two experiments.

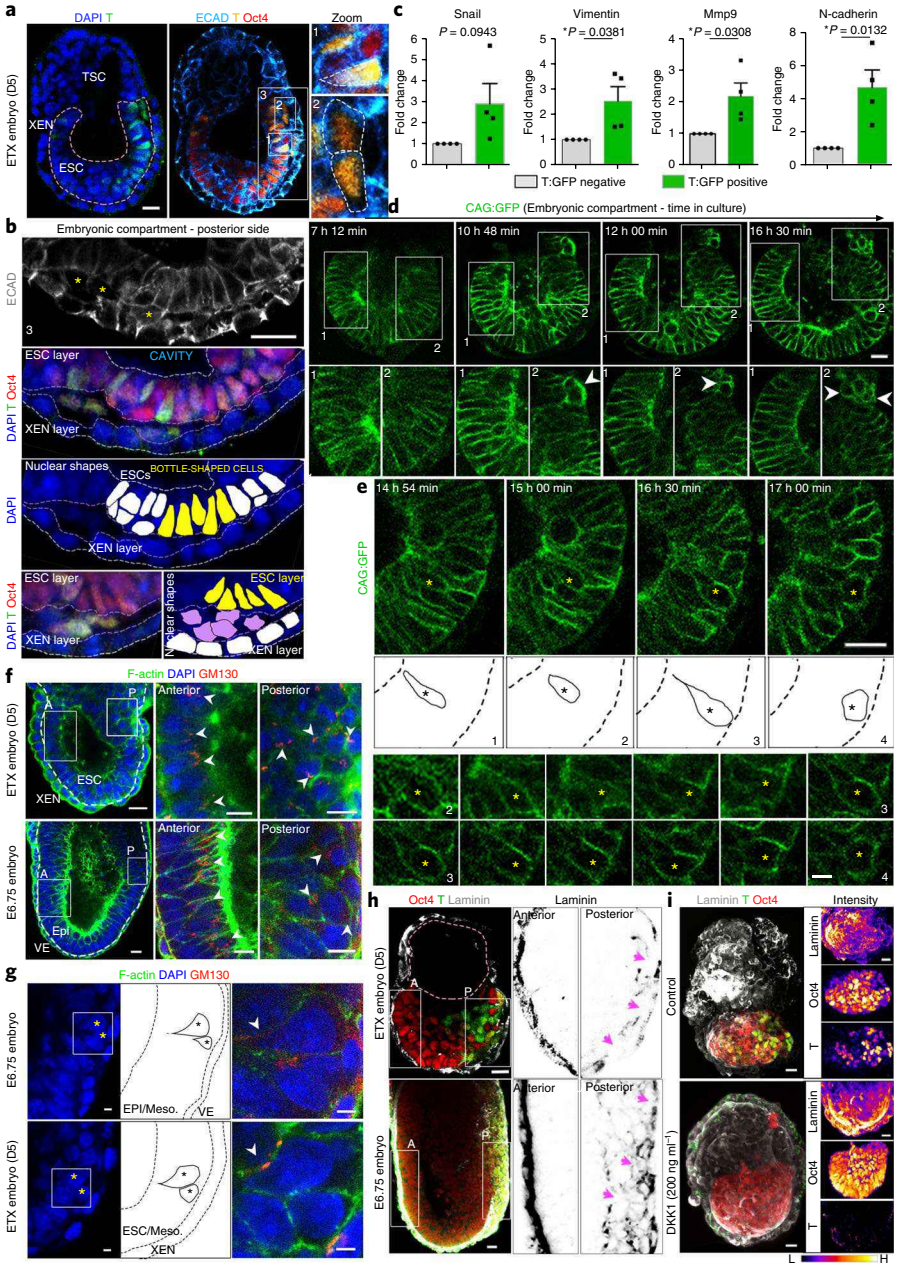

Fig. 4 | Epithelial-to-mesenchymal transition events in gastrulating ETX embryos. a, *T/Brachyury* expression in nascent mesoderm. Dashed line outlines the region of interest, the ES compartment. Magnified images: 1, Bottle-shaped *T/Brachyury*-positive cell (dashed lines); 2, Reoriented *T/Brachyury*-positive mesenchymal cells between the ES/XEN layers (dashed lines). Ten ETX embryos, four experiments. Scale bar, 20 μm. **b**, Boxed area 3 from **a**: posterior side of the ES compartment magnified and rotated 90°. Top: Asterisks indicate reoriented mesenchymal cells between ES/XEN layers. ECAD, E-cadherin. Scale bar, 20 μm. Second row: White dashed lines indicate border of ES/XEN layers; purple dashed lines outline cells between layers. Third row: Superimposed schematic—bottle-shaped ES cells (yellow) interspersed between epithelial cells (white). Bottom: Different focal plane shows repositioned T-positive cells (purple) between the ES/XEN layers. **c**, RT–qPCR of candidate EMT genes performed on cell extracts of day 5 ETX embryos (see Methods). Two-sided Student's *t*-test; means ± s.e.m. $n = 4$ biological replicates. **d**, Stills from time-lapse movie of live ETX embryo built from CAG:GFP ES cells. Cells on one side of the ES compartment (1, prospective anterior) maintain epithelial integrity. Cells on the opposite side (labelled 2, prospective posterior) reorient at the ES–TS boundary (arrowheads). Boxes show magnified fields at each time point. Three separate movies, seven ETX embryos. Scale bar, 20 μm. **e**, Top: Magnified stills of ES compartment revealing a cell (asterisks) undergoing apical constriction. Second row: 1–4, tracings of stills in top row. Third/fourth rows: Tracking of the same cell illustrating epithelial–bottle–mesenchymal shape change between 15 h 00 min (2), 16 h 30 min (3) and 17 h 00 min (4) time points. Scale bar, 5 μm. **f**, Polarized Golgi in anterior indicating epithelial integrity (arrowheads); asymmetrically distributed Golgi within mesenchymal cells on posterior. Dashed lines, embryonic compartment. 12 ETX embryos, three E6.75 natural embryos, four experiments. Scale bars, 20 μm. Scale bar in zoomed images, 10 μm. **g**, Magnified images from posterior shown in **f**. Migratory bottle cells are losing epithelial polarity (asterisks, left and middle; arrowheads, right). Scale bars, 5 μm. **h**, Laminin breakdown on *T/Brachyury*-expressing posterior. White boxes, magnified regions. Purple dashed lines, TS-derived extra-embryonic compartment. Rightmost panels, laminin staining inverted for better contrast of magnified regions. Purple arrows, laminin breakdown. Non-nuclear anti-*T/Brachyury* VE fluorescence represents non-specific staining. Scale bars, 20 μm. 15 ETX embryos, four experiments; six E6.75 embryos, two experiments. **i**, Day 5 ETX embryo with/without DKK1-treatment (200 ng ml^{-1}) for 24 h. Right, Maximum projections of ES compartments, pseudocoloured to highlight intensity gradients. Scale bar, 20 μm. 20 ETX embryos per group, two experiments.

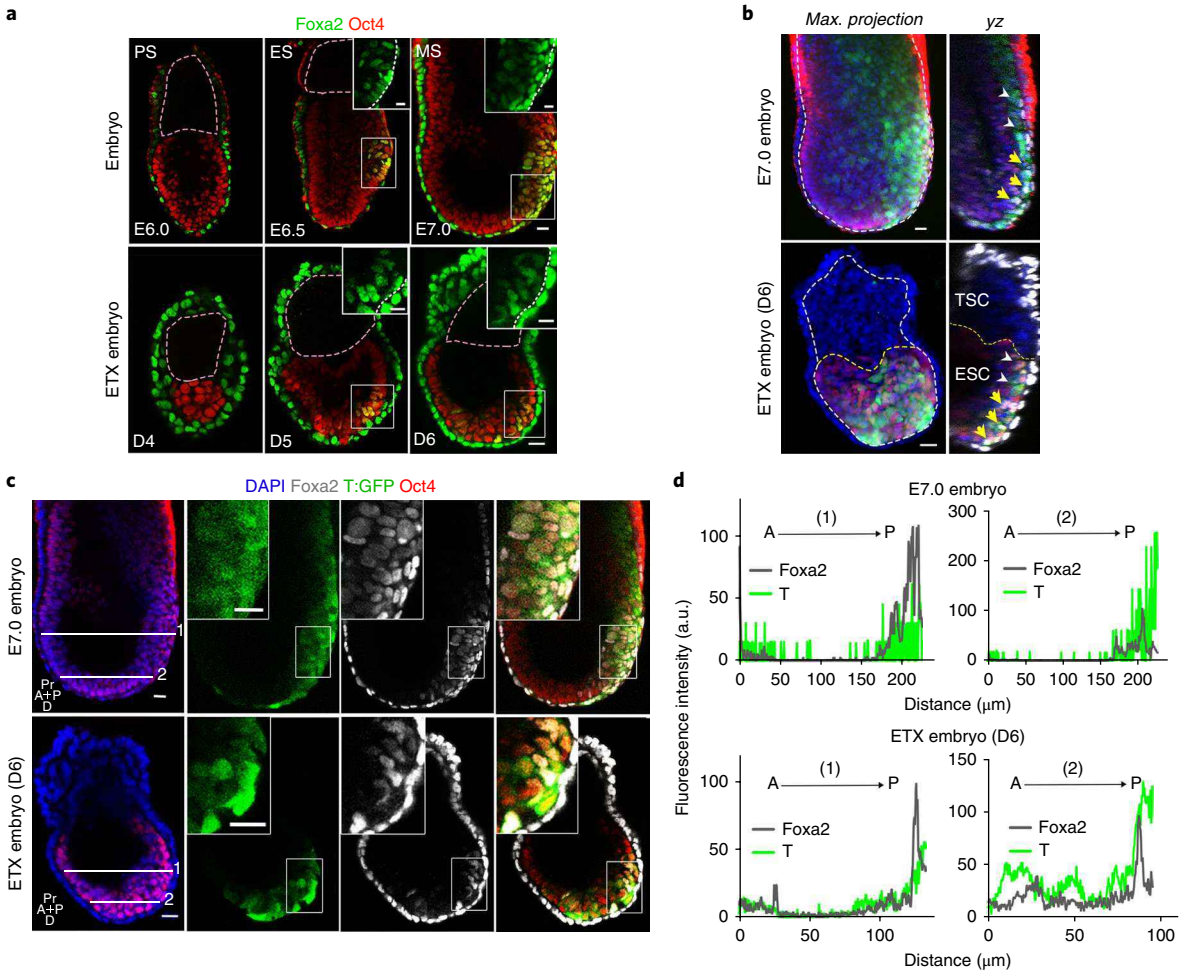

Fig. 5 | Spatio-temporal specification of axial mesoderm in gastrulating ETX embryos. a, Top, Mid-sagittal confocal sections of pre-streak (PS) E6.0, early streak (ES) E6.5 and mid-streak (MS) E7.0 stage embryo. Bottom, Mid-sagittal confocal sections of ETX embryos at days 4, 5 and 6. Immunostaining of Foxa2 reveals axial mesoderm specification. White boxes indicate region of magnified inset. Purple dashed lines outline ExE- or TS-cell-derived extra-embryonic compartment, for clarity. Scale bars, 20 μm. 20 ETX embryos, three experiments; 15 embryos, two experiments. **b**, E7.0 embryo and day 6 gastrulating ETX embryo presented in **a**. Left, Maximum projection images show *T*:GFP-positive posterior domain expanding from the embryonic/extra-embryonic boundary (yellow dashed lines) to distal tip of embryonic compartment. White dashed lines outline VE or XEN layer. Right, *yz* orthogonal views provided to visualize posterior domain. White arrowheads indicate *T*:GFP-positive cells on the boundary; yellow arrows indicate *T*:GFP-Foxa2 double positive mesoderm cells marking axial mesoderm induction on intermediate posterior domain. Ten natural embryos, three experiments; ten ETX embryos, three experiments. **c**,**d**, Single plane images (**c**). White boxes indicate region of magnified insets showing Foxa2-T double positive cells. White lines indicate two separate planes (marked 1 and 2) used to plot intensity profiles of *T*:GFP and Foxa2 fluorescence within epiblast/ES-compartment (**d**). Pr, proximal; D, distal; A, anterior; P, posterior. Ten natural embryos, three experiments; ten ETX embryos, three experiments. Scale bars, 20 μm.

and VE during gastrulation[20]. When we analysed ETX embryos developing to day 5 we could identify bottle-shaped *T/Brachyury*-expressing cells with nuclei oriented parallel rather than perpendicular to the basal membrane within the ES-derived embryonic compartment and between the ES and XEN layers (Fig. 4a,b and Supplementary Fig. 5a). To examine if these cells indeed had characteristics of migratory mesenchyme, we microsurgically isolated *T*:GFP-negative and T:GFP-positive cells and carried out RT–qPCR. This revealed upregulation of EMT markers *Snai1*, *Vimentin*, *Mmp9* and *N-cadherin* in *T*:GFP-positive cells (Fig. 4c), a transcriptional program reflecting the EMT.

To further confirm that such cells behaved as migrating mesenchyme, we next built ETX embryos using CAG:GFP ES cells and filmed their development. At the onset of *T/Brachyury* induction at day 4.5, CAG:GFP expressing ES cells on one side maintained intact, organized epithelium, whereas on the opposite side, they changed their orientation at the ES/TS boundary (arrowheads, Fig. 4d, Supplementary Fig. 5b). We could identify cells undergoing apical constriction within the ES cell layer and transitioning through a bottle- to a rounded-mesenchymal shape (asterisks, Fig. 4e; Supplementary Movie 2), supporting observations on fixed synthetic embryos and mirroring natural development[20]. We confirmed cell polarity changes in the posterior ES-derived embryonic compartment through loss of the apical positioning of the Golgi marker GM130, as cells adopted their bottle-shaped, migratory morphology (asterisk, Fig. 4f,g). Finally, newly formed mesenchymal cells also changed polarity from an apico-basal to a front–rear orientation, in a manner not due to the rounding of mitotic cells (Supplementary Fig. 5c,d). Reoriented cells in this newly formed mesoderm layer expressed N-cadherin but did not form a continuous epithelium (Supplementary Fig. 5e). These observations suggest that *T/Brachyury*-expressing cells in ETX embryos can undertake migratory events typical of the EMT.

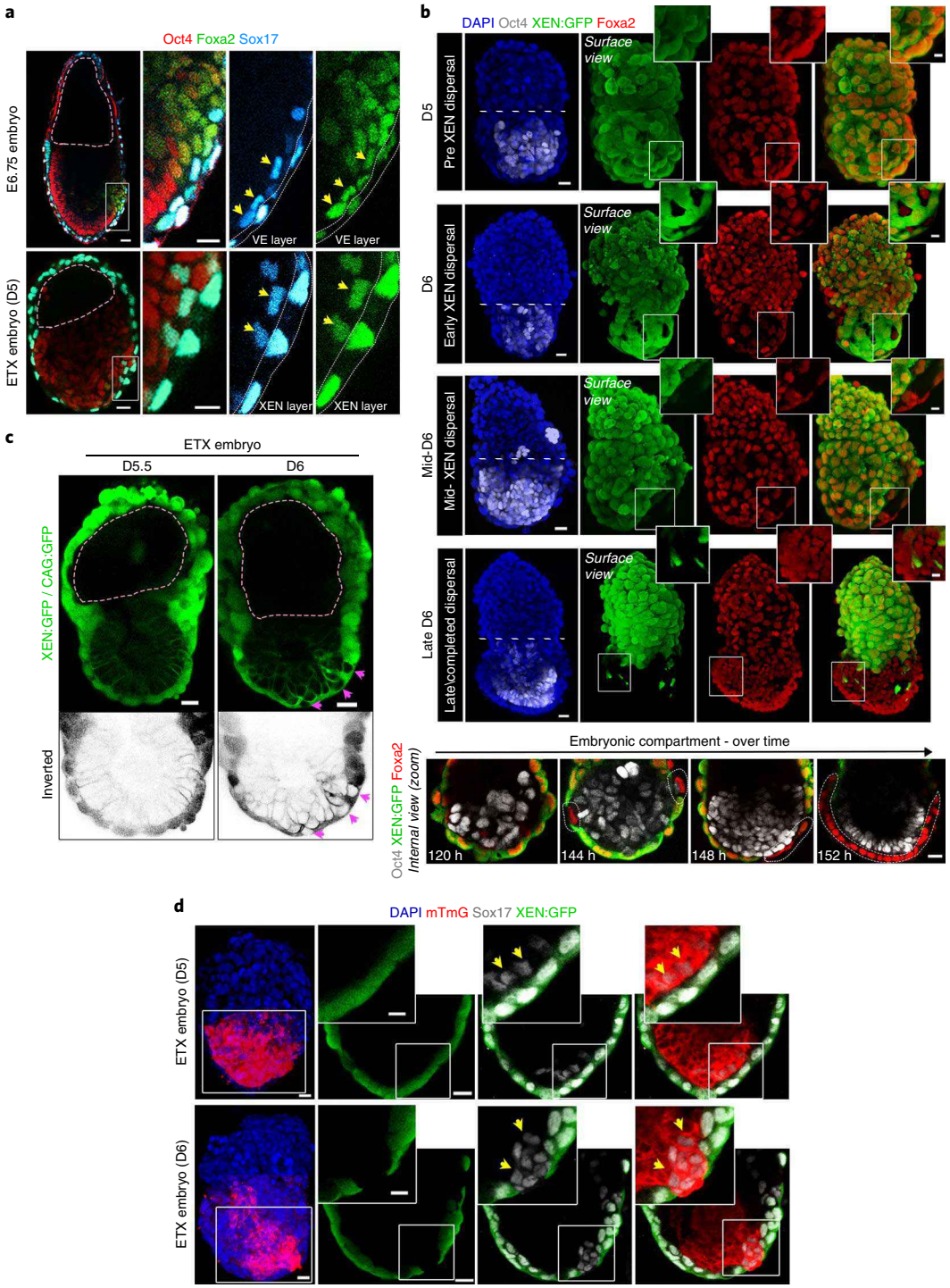

Fig. 6 | Spatio-temporal formation of definitive endoderm in gastrulating ETX embryos. a, Magnified fields (white boxes) indicate a subset of Foxa2–Sox17 double positive definitive endoderm cells (yellow arrows) in the process of egression within the epiblast/ES-cell layer and making contact with the embryonic emVE/emXEN layer (white dotted lines). Purple dashed lines outline ExE- or TS-derived extra-embryonic compartment, for clarity. Non-nuclear anti-Oct4 VE fluorescence represents non-specific binding. Scale bars, 20 μm. Four synthetic embryos; three embryos, two experiments. **b**, XEN:EGFP reporter ETX embryos at day 5 (10 embryos), day 6 (10 embryos) and mid/late day 6 (6 embryos) showing progressive XEN cell dispersal. White boxes indicate zoomed insets. Magnified insets in the second row show the rotated *x* axis for better visualization. White dashed lines mark embryonic/extra-embryonic boundary. Lower panel, White dashed lines outline cells egressed into the EGFP-positive XEN layer. Scale bars, 20 μm. Four experiments. **c**, Images from live ETX embryos generated from CAG:GFP ES, EGFP XEN and wild-type TS cells at indicated stages. Purple arrows: intercalated ES cells in the XEN layer. GFP-labelled embryonic compartments are inverted for better contrast of the zoomed inset (bottom). Purple dashed lines outline ExE- or TS-cell-derived extra-embryonic compartment, for clarity. Scale bars, 20 μm. Ten embryos per time point. **d**, EGFP XEN and mTmG ES cell reporter ETX embryos at days 5 and 6 showing progression of ES cell intercalation in the XEN layer. White boxes indicate the region of the magnified insets. Yellow arrows show Sox17 upregulation in presumptive definitive endoderm cells within the mTmG-labelled ES cell compartment in the process of egression (upper) or having egressed (lower) into the XEN:EGFP layer. Three embryos per time point, two experiments. Scale bars, 20 μm; in row of zoomed images, 10 μm.

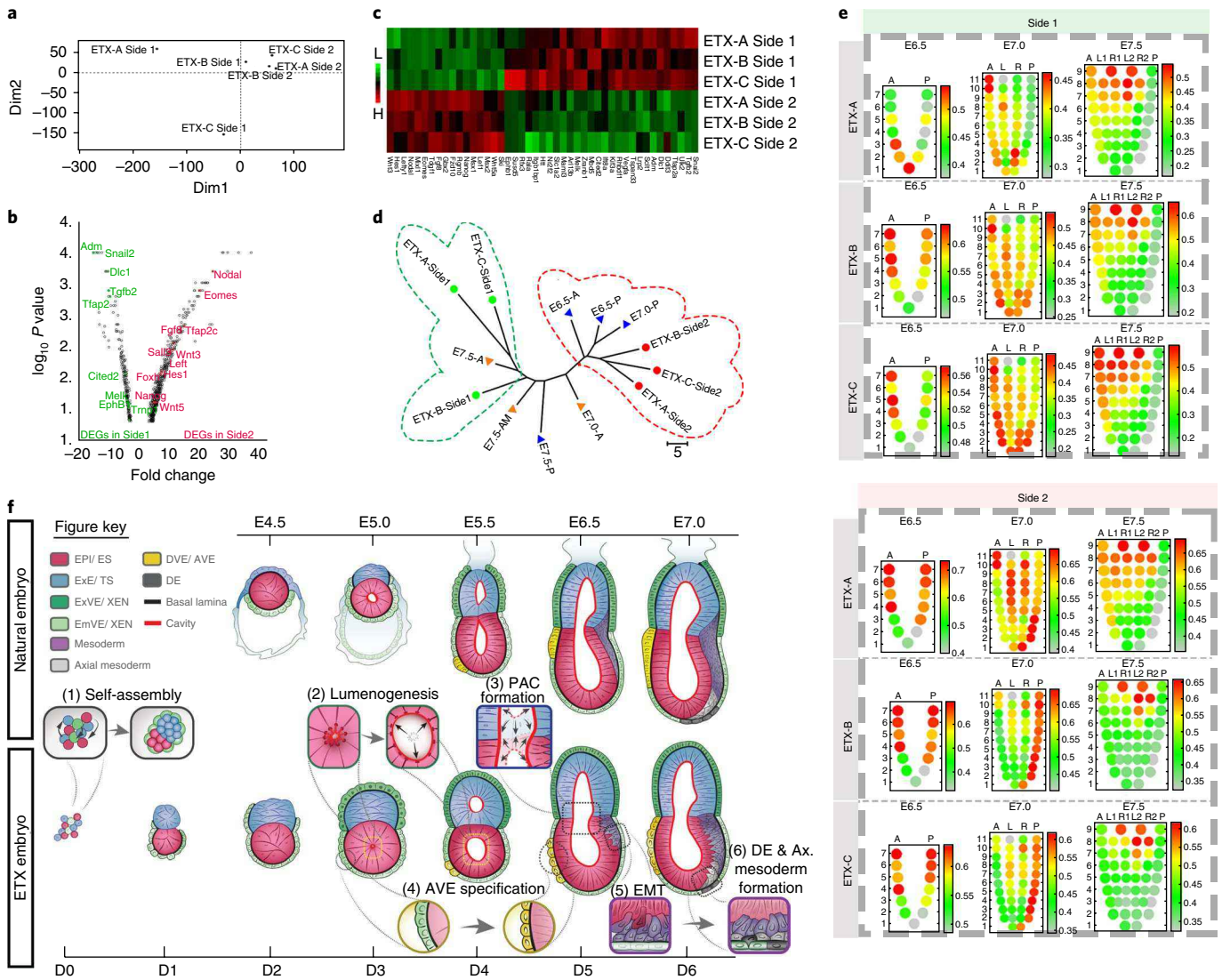

Fig. 7 | Transcriptional profiling of gastrulating ETX embryos reveals global similarity of anterior–posterior patterning to gastrulating natural embryos. **a**, PCA of the transcriptome from each side (side 1, prospective anterior versus side 2, prospective posterior) of each gastrulating ETX embryo (ETX-A, ETX-B and ETX-C). $n=3$ biological replicates, divided into side 1 and side 2. **b**, Volcano plot showing DEGs in side 1 and side 2 of gastrulating ETX embryos. Plotted genes have $P<0.05$ and fold change of >1.5. Red dots: selected genes required for posterior development. Green dots: genes required for anterior development. $n=3$ biological replicates, divided into side 1 and side 2. **c**, Heatmap showing expression of 45 selected genes in each side of each ETX embryos. Highest expression, dark red; lowest, dark green. **d**, NJ tree inferring phylogenetic trajectories of side 1 and 2 transcriptomes of gastrulating ETX embryos and anterior and posterior parts of natural embryos (see Methods). Green dashed lines outline clustered samples showing anterior identity; red dashed lines outline clustered samples showing posterior identity. **e**, Corn plots representing the Pearson correlation coefficient (PCC) between transcriptomes from each side of gastrulating ETX embryos ($n=3$ biological replicates, divided into side 1 and side 2) and spatial domains of natural embryo epiblast at different developmental timepoints ($n=13$ E6.5, $n=42$ E7.0, $n=46$ E7.5). Stage of natural embryo development indicated by the corn plots. Numbers on the left side of the corn plots indicate each laser capture microdissection (LCM) sample collected from along the proximal–distal axis of the mouse epiblast (see Methods) (that is, 1 indicates LCM sample from the distal tip of the epiblast, whereas the largest number in the series for a given corn plot indicates LCM sample from the embryonic–extra-embryonic boundary). Right-hand colour scale indicates magnitude of PCC. Red indicates highest correlation; grey, no correlation. Transverse sections of natural embryos were collected along the proximal–distal axis and divided into subdomains. A, anterior; P, posterior; L, left; R, right. **f**, Schematic representation of our findings comparing development of a gastrulating ETX embryo (bottom) with a natural embryo (top). EMT, epithelial-to-mesenchymal transition; DE, definitive endoderm; Ax: axial (mesoderm); PAC: pro-amniotic cavity.

To achieve ingression during the EMT, cells have to breach the basement membrane[20,21]. To determine if this occurs in ETX embryos, we analysed the major component of basement membrane, laminin. We found laminin was disrupted in the region of *T/Brachyury* expression (Fig. 4h and Supplementary Fig. 5f,g). To determine whether this disruption depended on Wnt signalling, as is the case during natural embryogenesis, we subjected ETX embryos to the Wnt antagonist, DKK1. This prevented *T/Brachyury* expression and basement membrane disruption (Fig. 4i, Supplementary Fig. 5h, 70% versus 25%, $P<0.05$ Fisher's exact test, $n=20$ ETX embryos per group). Thus, ETX embryos can undertake the migratory events of the EMT and therefore gastrulate.

Axial mesoderm and definitive endoderm development. In natural development, the EMT and mesoderm specification are followed by mesoderm patterning, so we next determined whether

mesoderm in gastrulating embryo-like structures could develop to express axial mesodermal markers. We found that Foxa2, a transcription factor also expressed later in definitive endoderm[22,23], was expressed in XEN cells and a cluster of intermediate posterior ES cells at day 5, resembling early axial mesoderm induction 6.5 days after fertilization (Fig. 5a, middle). Cells expressing both Foxa2 and *T/Brachyury* were at the most distal part of the posterior domain at day 6 (Fig. 5a–d and Supplementary Fig. 6a,b). This expression pattern is typical of cells fated to become axial mesoderm, confined to the anterior-most primitive streak in E7.0 embryos[24] (Fig. 5a–d and Supplementary Fig. 6a,b) and which will then express genes identifying the notochord and node[25]. Thus, progression of mesoderm development in gastrulating embryo-like structures appears similar to natural embryos.

In natural embryos, definitive endoderm cells emerging from the anterior primitive streak become incorporated into the VE, which is progressively displaced anteriorly and proximally[15]. We found that similar events can be achieved in gastrulating ETX embryos, as we observed a subset of Foxa2- and Sox17-expressing cells between the ES and XEN compartments and contacting the XEN layer at day 5 (Fig. 6a). To substantiate these observations, we built ETX embryos with EGFP-reporter XEN cells. Strikingly, as development progressed, GFP-negative areas appeared in the continuous layer of GFP-positive XEN cells at day 6, as egressing cells from the ES-derived compartment were accommodated there (Fig. 6b, second row). Accordingly, cells in these GFP-negative areas expressed the definitive endoderm marker Foxa2 (Fig. 6b, second and third row). By the end of day 6, there were few remaining GFP-positive cells, suggesting ES-derived definitive endoderm cells had largely replaced the XEN-derived VE-like layer (Fig. 6b, fourth row). To confirm this further, we built ETX embryos using XEN:GFP cells and membrane-marked CAG:GFP or mTmG ES cells (Fig. 6c,d). Again, we found egressing Sox17-positive mTmG cells that contacted the XEN layer at day 5 and intercalated into the XEN layer at day 6 (Fig. 6d). These results demonstrate that gastrulating ETX embryos develop not only mesoderm but also definitive endoderm.

Gastrulating embryo-like structures resemble E7.0 mid-gastrula embryos in gene expression. Finally, we sought to compare gene expression patterns between gastrulating ETX embryos and natural embryos. We therefore built ETX embryos from *T*:GFP-expressing ES cells and dissected at day 5 their individual non-fluorescent prospective anterior parts (side 1) and fluorescent prospective posterior parts (side 2) to isolate mRNA for deep RNA–seq (see Methods). Principal component analysis (PCA) indicated close clustering of side 2 and more loose clustering, or higher variability, in side 1 (Fig. 7a and Supplementary Fig. 7a–c), indicating distinct patterning between the two sides.

We identified 499 genes upregulated on side 2 compared to side 1 and 239 upregulated on side 1 compared to side 2, with good agreement between biological replicates (Fig. 7b,c and Supplementary Fig. 7a–c). Gene ontology (GO) analysis of genes upregulated on side 1 identified terms associated with anterior embryonic development, including neural precursor and nervous system development, whereas side 2 analysis identified terms relevant to posterior development including gastrulation, node formation, cilium assembly and left–right symmetry (Fig. 7c and Supplementary Fig. 7c–e). Moreover, genes differentially expressed on side 2 included posterior fate determinants such as Nodal, Wnt, Eomes, Mixl1 and Nanog (Fig. 7b,c). Thus side 1 of gastrulating ETX embryos had an anterior, and side 2, a posterior gene expression signature.

To further assess developmental relationships of gastrulating ETX embryos and the anterior/posterior parts of natural embryos, we performed a neighbour-joining (NJ) tree analysis[26] to generate a gene signature for different sample domains using differentially expressed genes (DEGs) to compute topological distances and a distance matrix. These signatures allowed us to group ETX embryos and the epiblast of natural embryos at E6.5, E7.0 and E7.5 into a phylogenetic tree whose branching indicates samples most similar in gene expression (Fig. 7d). All side 2 samples of ETX embryos clustered closely with the posterior part of the E7.0 embryo, and side 1 samples with the anterior part of the E7.5 embryo, supporting the idea that axis patterning of gastrulating ETX embryos occurs as in natural embryos (Fig. 7d).

Having identified such an anterior signature for side 1 and posterior signature for side 2, we next wished to compare the side 1 and 2 transcriptomes to spatial domains of gene expression in the epiblast of embryos. To this end, we calculated the correlation between gene expression levels from side 1 or side 2 samples from three gastrulating ETX embryos (A, B, C; Fig. 7e) and particular epiblast regions at E6.5, E7.0 and E7.5, visualizing the outcome on 'corn plots'[27]. Side 2 samples of gastrulating ETX embryos showed few regionalized differences with E6.5 embryos, but strongly resembled the posterior of gastrulating embryos at E7.0 (Fig. 7e). This correlation of posterior gene expression between side 2 of ETX embryos and E7.5 embryos was not evident. Side 1 samples of ETX embryos showed very weak correlation in gene expression pattern with the anterior epiblast of E6.5 embryos and an increasingly striking correlation with the anterior subdomains of the epiblast at E7.0 and E7.5 (Fig. 7e). Thus, the transcriptomes of sides 1 and 2 of ETX embryos correlate with the respective anterior and posterior epiblast of gastrulating embryos, supporting the conclusion that ETX embryos develop to specify regionalized domains characteristic of natural gastrulation.

Discussion

Here, we describe the ability of the stem cell types derived from the three component tissues of the mouse embryo to collaborate to form structures that morphologically and transcriptionally resemble embryos developing to exhibit key landmarks of gastrulation, including mesoderm and definitive endoderm formation. In this model system, we have made no attempt to direct stem cells to cooperate, but have allowed them to self-sort and self-organize. Thus, it is remarkable that many (although not all) of the resulting multicellular aggregates develop to resemble gastrulating natural embryos in both morphology and gene expression. We conclude that the ability for such a large proportion of ETX embryos to form spontaneously reflects the robust self-organizing properties of mammalian development.

Some features of the gastrulating ETX embryo model we describe here were also seen in our previous ET embryo model comprising only ES and TS cells[3]. As with ET embryos, ETX embryos form distinct, ES-derived and TS-derived compartments that undertake lumenogenesis and then form a common cavity resembling the pro-amniotic cavity of natural pre-gastrulating embryos. They then take the next step and specify mesoderm, as shown by *T/Brachyury* expression in the embryonic-like compartment abutting the extra-embryonic boundary (Fig. 7f). Moreover, both synthetic ET and ETX embryos initiate PGC-like cell formation in the proximal-most part of this *T/Brachyury* domain. However, whereas development of ET embryos requires exogenous extracellular matrix, as we have previously shown[3], the XEN-derived VE-like layer in the ETX embryos overcomes this requirement, permitting them to develop further (Fig. 7f). As synthetic embryogenesis progresses, this enveloping VE-like layer becomes regionalized, as in natural development. Also, within the squamous cells covering the embryonic-like compartment of some ETX embryos, we could observe an emerging group of cells expressing anterior signalling centre markers. The VE-like layer also permits the orderly morphogenetic events of gastrulation evident from the onset of EMT-associated gene expression as well as the shape changes and migration of *T/Brachyury*-expressing cells to create a cell layer between the ES-derived embryonic compartment and VE-like cells.

These *T/Brachyury*-expressing cells develop to express axial mesoderm markers and to migrate outwards to intercalate into the VE-like layer to form cells resembling definitive endoderm. Our results also show that at this stage, cells from the anterior and posterior parts of the gastrulating ETX embryos exhibit gene expression characteristic of natural gastrulating embryos at E7.0/E7.5 of development.

The gastrulation of ETX embryos is not perfect. We do not, for example, observe the formation of mesodermal wings as during natural gastrulation. Cell ingression into the mesodermal layer is also not uniform along the *T/Brachyury*-positive domain. Thus, although the ETX embryos are gastrulating, the final structures are incomplete. However, it is important to note that even natural embryos do not gastrulate in vitro as perfectly as embryos developing in vivo. Nevertheless, despite this current limitation, our results show that the principal morphogenetic events of the early/mid stages of gastrulation in vivo can occur in the correct spatio-temporal sequence in ETX embryos established from three stem cell types in vitro.

In conclusion, the results we present here demonstrate the remarkable self-organizing ability of the three distinct stem cell types for the three founding tissues to build embryo-like structures that recapitulate not only embryo morphogenesis and gene expression but also, uniquely, the gastrulation cell movements leading to axial mesoderm and definitive endoderm specification.

Received: 18 April 2018; Accepted: 20 June 2018;
Published online: 23 July 2018

References

1. Bedzhov, I. & Zernicka-Goetz, M. Self-organizing properties of mouse pluripotent cells initiate morphogenesis upon implantation. *Cell* **156**, 1032–1044 (2014).
2. Shahbazi, M. N. et al. Pluripotent state transitions coordinate morphogenesis in mouse and human embryos. *Nature* **552**, 239–243 (2017).
3. Harrison, S. E., Sozen, B., Christodoulou, N., Kyprianou, C. & Zernicka-Goetz, M. Assembly of embryonic and extraembryonic stem cells to mimic embryogenesis in vitro. *Science* **356**, eaal1810 (2017).
4. Rivera-Perez, J. A. & Magnuson, T. Primitive streak formation in mice is preceded by localized activation of Brachyury and Wnt3. *Dev. Biol.* **288**, 363–371(2005).
5. Robertson, E. J. Dose-dependent Nodal/Smad signals pattern the early mouse embryo. *Semin. Cell Dev. Biol.* **32**, 73–79 (2014).
6. Wood, S. A., Allen, N. D., Rossant, J., Auerbach, A. & Nagy, A. Non-injection methods for the production of embryonic stem cell-embryo chimaeras. *Nature* **365**, 87–89 (1993).
7. Bradley, A., Evans, M., Kaufman, M. H. & Robertson, E. Formation of germ-line chimaeras from embryo-derived teratocarcinoma cell lines. *Nature* **309**, 255–256 (1984).
8. ten Berge, D. et al. Wnt signaling mediates self-organization and axis formation in embryoid bodies. *Cell Stem Cell* **3**, 508–518 (2008).
9. van den Brink, S. C. et al. Symmetry breaking, germ layer specification and axial organization in aggregates of mouse embryonic stem cells. *Development* **141**, 4231–4242 (2014).
10. Warmflash, A., Sorre, B., Etoc, F., Siggia, E. D. & Brivanlou, A. H. A method to recapitulate early embryonic spatial patterning in human embryonic stem cells. *Nat. Methods* **11**, 847–854 (2014).
11. Tanaka, S., Kunath, T., Hadjantonakis, A. K., Nagy, A. & Rossant, J. Promotion of trophoblast stem cell proliferation by FGF4. *Science* **282**, 2072–2075 (1998).
12. Kimura-Yoshida, C. et al. Canonical Wnt signaling and its antagonist regulate anterior–posterior axis polarisation by guiding cell migration in mouse visceral endoderm. *Dev. Cell* **9**, 639–650 (2005).
13. Yamamoto, M. et al. Nodal antagonists regulate formation of the anteroposterior axis of the mouse embryo. *Nature* **428**, 387–392 (2004).
14. Tam, P. P., & Beddington, R. S. Establishment and organization of germ layers in the gastrulating mouse embryo. *Ciba Found. Symp.* **165**, 27–42 (1992).
15. Viotti, M., Nowotschin, S. & Hadjantonakis, A. K. Afp::mCherry, a red fluorescent transgenic reporter of the mouse visceral endoderm. *Genesis* **49**, 124–133 (2011).
16. Kunath, T. et al. Imprinted X-inactivation in extra-embryonic endoderm cell lines from mouse blastocysts. *Development* **132**, 1649–1661 (2005).
17. Takaoka, K., Yamamoto, M. & Hamada, H. Origin and role of distal visceral endoderm, a group of cells that determines anterior-posterior polarity of the mouse embryo. *Nat. Cell Biol.* **13**, 743–752 (2011).
18. Papanayotou, C. et al. A novel nodal enhancer dependent on pluripotency factors and smad2/3 signaling conditions a regulatory switch during epiblast maturation. *PLoS Biol.* **12**, e1001890 (2014).
19. Hoshino, H., Shioi, G. & Aizawa, S. AVE protein expression and visceral endoderm cell behavior during anterior-posterior axis formation in mouse embryos: asymmetry in OTX2 and DKK1 expression. *Dev. Biol.* **402**, 175–191 (2015).
20. Williams, M., Burdsal, C., Periasamy, A., Lewandoski, M. & Sutherland, A. Mouse primitive streak forms in situ by initiation of epithelial to mesenchymal transition without migration of a cell population. *Dev. Dyn.* **241**, 270–283 (2012).
21. Laurie, G. W., Leblond, C. P. & Martin, G. R. Localization of type IV collagen, laminin, heparan sulfate proteoglycan, and fibronectin to the basal lamina of basement membranes. *J. Cell Biol.* **95**, 340–344 (1982).
22. Sasaki, H. & Hogan, B. L. Differential expression of multiple fork head related genes during gastrulation and axial pattern formation in the mouse embryo. *Development* **118**, 47–59 (1993).
23. Lewis, S. L. & Tam, P. P. Definitive endoderm of the mouse embryo: formation, cell fates, and morphogenetic function. *Dev. Dyn.* **235**, 2315–2329 (2006).
24. Burtscher, I. & Lickert, H. Foxa2 regulates polarity and epithelialization in the endoderm germ layer of the mouse embryo. *Development* **136**, 1029–1038 (2009).
25. Balmer, S., Nowotschin, S. & Hadjantonakis, A. K. Notochord morphogenesis in mice: current understanding & open questions. *Dev. Dyn.* **245**, 547–557 (2016).
26. Saitou, N. & Nei, M. The neighbor-joining method: a new method for reconstructing phylogenetic trees. *Mol. Biol. Evol.* **4**, 406–425 (1987).
27. Peng, G. et al. Spatial transcriptome for the molecular annotation of lineage fates and cell identity in mid-gastrula mouse embryo. *Dev. Cell* **36**, 681–697 (2016).

Acknowledgements

The authors thank colleagues in the M.Z.G. laboratory for insightful comments. The M.Z.G. laboratory is supported by grants from the European Research Council (669198) and the Wellcome Trust (098287/Z/12/Z). B.S. is also supported by Akdeniz University, Turkey. T.V. and L.C. are funded by Wellcome. T.V. is also funded by the University of Leuven, Belgium (PFV/10/016). The authors thank A. Weberling, M. Mole, N. Christodoulou, C. Kyprianou and J. Guo for their help, A. Hupalowska for inspiration for a model in Fig. 7f, and L. Wittler, I. Urban, A. Landsberger, C. Schick and H. Schlenger for technical support.

Author contributions

B.S., G.A. and A.C. with the help of S.C. carried out experiments and data analysis. R.W. and N.J. analysed the sequencing data. E.N. and G.M. contributed to stem cell derivation and the experimental design. L.C. prepared cDNA libraries. T.V. supervised the cDNA library preparation. D.M.G. co-supervised parts of the study. M.Z.G. conceived and supervised the study, and wrote the paper with the help of B.S., G.A. and D.M.G.

Additional information

Supplementary information is available for this paper at https://doi.org/10.1038/s41556-018-0147-7.

Reprints and permissions information is available at www.nature.com/reprints.

Correspondence and requests for materials should be addressed to M.Z.

Publisher's note: Springer Nature remains neutral with regard to jurisdictional claims in published maps and institutional affiliations.

Methods

Embryo recovery and culture. Mice were kept in the animal house in accordance with national and international guidelines. All experiments were regulated by the Animals (Scientific Procedures) Act 1986 Amendment Regulations 2012 following ethical review by the University of Cambridge Animal Welfare and Ethical Review Body (AWERB). Experiments were approved by the Home Office. Animals were inspected daily and those that showed health concerns were culled by cervical dislocation.

Six-week-old female CD-1 mice were naturally mated and killed after 5, 6 or 7 days post coitum. The uterus was recovered and embryos dissected from deciduae in M2 medium. Blastocysts were recovered at E4.5 by uterine flushing, their mural trophectoderm dissected away, then cultured in IVC1 and IVC2 media (Cell Guidance Systems), as previously decribed[28].

Cell culture. ES and TS cells were cultured at 37 °C in 5% CO_2 on mitotically inactivated CF1 or NMRI mouse embryonic fibroblasts (MEFs) and passaged once they reached 80% confluency. Cells were cultured in ETX medium consisting of Dulbecco's modified essential medium (DMEM, Gibco cat. no. 21969) with 12.5% FBS, 2 mM GlutaMax (Gibco cat. no. 35050-038), 0.1 mM 2-mercaptoethanol (2-ME, Gibco cat. no. 31350-010), 0.1 mM nonessential amino acids (Gibco cat. no. 11140-035), 1 mM sodium pyruvate (Gibco cat. no. 11360-039), 0.02 M HEPES (Gibco cat. no. 15630080) and 1% penicillin–streptomycin (Gibco cat. no. 15140122); ESC medium was supplemented with PD0325901 (1 mM), CHIR99021 (3 mM, 2i) and leukaemia inhibitory factor (0.1 mM, LIF) (ETX-2iLIF). TSC medium was supplemented with FGF2 (25 ng ml^{-1}; Peprotech), FGF4 (25 ng ml^{-1}; Peprotech) and heparin (1 µg ml^{-1}; Sigma) (ETX-F42H). XEN cells were cultured on gelatinized tissue-culture-grade plates, in 70% MEF-conditioned ETX medium (C-ETX), without any additional supplements.

Cell lines. Experiments were performed using mouse wild-type ES cells, Nodal HBE-YFP ES cells[18], *T*:GFP ES cells[29], CAG:GFP ES cells[30], wild-type TS cells, wild-type XEN cells and EGFP XEN cells. Wild-type TS cells were a gift from J. Nichols (University of Cambridge) and EGFP XENs were a gift from P. Rugg-Gunn (Babraham Institute).

Preparing and plating cell suspensions for 'AggreWell' aggregation experiments. The full protocol was repeated independently in the University of Cambridge, Charité University and MaxPlanck Institute in Berlin, and is available on Protocol Exchange[31].

For AggreWell plate preparation, the manufacturer's protocol was followed. Briefly, wells were rinsed with rinsing solution (Stem Cell Technologies), centrifuged for 5 min at 2,000*g* and incubated at room temperature in the tissue culture hood for 20 min. After incubation, the wells were washed with 2 ml of 1× PBS. After PBS removal, 500 µl of filtered C-ETX medium was added to each well and the plate was spun for 5 min at 2,000*g* and then placed at 37 °C in 5% CO_2 until ready to use.

ES and TS cell colonies were dissociated to single cells by incubation with 0.05% trypsin-EDTA at 37 °C for 3 min. Cells were pelleted by centrifugation for 4 min at 1,000 r.p.m. and resuspended in MEF-conditioned ETX medium (C-ETX, as above). Cell suspension was pre-incubated at 37 °C in 5% CO_2 on gelatinized tissue-culture-grade plates for 30 min to remove MEFs until re-collection of ES and TS cell suspensions. Meanwhile, XEN cells were dissociated to single cells by incubation with 0.05% trypsin-EDTA at 37 °C for 3 min, and pelleted by centrifugation for 4 min/1,000 r.p.m. and resuspended in C-ETX medium. A total of 7,200 ES cells per well, 19,200 TS cells per well and 5,400 XEN cells per well were counted using a haemocytometer. ES, TS and XEN cell suspensions were then mixed and repelleted. The cell mixture was resuspended in ETX medium (C-ETX medium) consisting of 70% MEF-conditioned DMEM with 12.5% FBS, 2 mM GlutaMax, 0.1 mM 2-mercaptoethanol (2-ME), 0.1 mM nonessential amino acids, 1 mM sodium pyruvate, 0.02 M HEPES, plus ROCK inhibitor (Y27632; Stemgent, 5 nM), and added dropwise to the well. The AggreWell plate was centrifuged for 3 min at 100*g*, outside wells were filled with PBS to prevent evaporation, and plates were placed at 37 °C and 5% CO_2. On the following day (day 1), 1 ml of medium from each well was slowly removed and replaced with 1 ml of fresh medium without ROCK inhibitor. This step was performed a second time to fully remove the ROCK inhibitor. On day 2, 1 mL of C-ETX medium was replaced with 1 mL of fresh medium. On day 3, the media was changed to IVC1 (Cell Guidance Systems) by removing 1.2 mL of media and replacing it with 1.5 mL of IVC1 medium. On day 4, IVC1 was replaced with IVC2 by removing 1.2 mL of media and replacing it with 1.5 mL of IVC2 (Cell Guidance Systems). On days 5 and 6, 1 mL of IVC2 was replaced with 1 mL of fresh IVC2.

Immunofluorescence staining. ETX and natural embryos were fixed in 4% paraformaldehyde for 20 min at room temperature, washed twice in PBT (PBS plus 0.05% Tween-20) and permeabilized for 30 min at room temperature in 0.3% Triton X-100, 0.1% glycin. Primary antibody incubation was performed overnight at 4 °C in blocking buffer (PBS plus 10% FBS, 1% Tween-20). The next day, embryos were washed twice in PBT, then incubated overnight with secondary antibody (1:500) in blocking buffer at 4 °C. On day 3, embryos were washed twice in PBT and incubated for 1 h at room temperature in 4′,6-diamidino-2-phenylindole (DAPI) plus PBT (5 mg ml^{-1}). Embryos were transferred to PBT drops in oil-filled optical plates before confocal imaging. For the antibodies used see Supplementary Table 1.

Criteria for ETX embryo inclusion and comparison to natural embryos. Following completion of any given aggregation experiment, ETX embryos were fixed (see 'Immunofluorescence staining') and those clearly displaying an outer layer of cells and two inner, well-defined compartments were manually selected for further analysis. Identity of the compartments was verified by immunofluorescence using Oct4 to mark the ES cell-derived embryonic compartment, Tfap2c or Eomes for the TS cell-derived, and Gata4, Gata6 or Sox17 for the XEN cell-derived extra-embryonic compartments. This was not necessary in instances where cell lines with appropriate fluorescent reporters were used.

ETX embryos were staged relative to natural embryos based on their common morphological features and developmental milestones. In a typical experiment, lumenogenesis was initiated at day 3 with only a single cavity present in the ES-derived embryonic compartment. This stage is comparable to E5.0/E5.25. By day 4, one or more small additional cavities developed within the TS-derived extra-embryonic compartment; this stage is comparable to an E5.5 stage natural embryo. By day 5, the cavities in the ES and TS compartments combined into a single large cavity, *T/Brachyury* was expressed and cell migratory events took place; this stage is comparable to an E6.0/E6.75 natural embryo. Finally, definitive endoderm and axial mesoderm formation in ETX embryos could be observed from day 6 onwards; this stage was comparable to a natural E6.75/E7.5 embryo.

Cryosectioning and immunostaining. ETX embryos and natural embryos were fixed for 20 min in 4% PFA at room temperature and washed twice in PBS. Samples were infiltrated in ice-cold 20% sucrose (in PBS) until each sample dropped to the bottom of a plate, embedded in 20% sucrose/7.5% gelatin (in PBS), and frozen in liquid nitrogen. Blocks were serially sectioned in the transverse plane at 15 µm thickness. Sections on slides were stored at −20 °C overnight. For immunostaining, sections were rehydrated for 10 min in PBS, permeabilized for 15 min in 0.1 M Glycin/0.3% Triton X-100, washed twice in PBS, blocked for at least 1 h, and then incubated with primary antibodies overnight at 4 °C. Sections were then washed twice in 0.5% Tween/PBS, incubated with secondary antibodies for 1 h at room temperature, washed twice in 0.5% Tween-20/PBS and mounted for confocal microscopy with ProLong Gold Antifade Mountant with DAPI. For antibodies used see Supplementary Table 1.

Image data acquisition, processing and quantification. Images were acquired with an inverted Leica SP8 confocal microscope (Leica Microsystems), using a Leica Fluotar VISIR 0.95 NA ×25 objective. Fluorophores were excited with a 405 nm diode laser (DAPI), a 488 nm argon laser (GFP), a 543 nm HeNe laser (Alexa Fluor 543/555) and a 633 nm HeNe laser (Alexa Fluor 633/647). Images were acquired with 0.5–1.2 µm *z* separation. Raw data were processed using open-source image analysis software Fiji or Imaris (Bitplane) and assembled in Photoshop CC 2017 (Adobe). Digital quantifications and immunofluorescence signal intensity graphs were obtained using Fiji software, and quantification of the cell number was performed in Imaris software.

Immunofluorescence intensity measurements of gene expression. For Nodal-YFP asymmetry, analysis was performed using Fiji software. A line from the proximal–distal axis, defining the midline of ETX embryos, was drawn to determine the left and right sides of the structure. Second, the shape of each nucleus in the embryonic compartment (Oct4 positive) was traced and added as a region of interest (ROI) to the ROI manager tool. The corresponding Nodal-YFP channel was then selected and all the previously defined ROIs were used to measure a mean intensity value in the Nodal-YFP channel for each cell nucleus. This procedure was repeated five times for other *z* planes. All the values for the left side were then plotted against all the values for the right side and tested with Student's *t*-test. ETX embryos were considered to express Nodal-YFP asymmetrically where statistically significant differences were shown between left and right.

For Lefty1 asymmetry, analysis was performed using Fiji software. A line from the proximal–distal axis, defining the midline of ETX embryos, was drawn to determine the left and right sides of the structure. For each selected *z* plane, a line was drawn from left to right of the ETX embryos, following the curvature of the XEN layer (XEN/VE markers). The grey values (intensities) for Lefty1 were calculated using the 'plot-profile' function. This measurement was performed on the right and left side of at least six *z* planes (see figure legends). If the average Lefty1 intensity was statistically significantly different between left and right sides (Student's *t*-test), Lefty1 was considered asymmetric.

Reconstruction of the embryonic compartment of ETX embryos and natural embryos. Reconstruction was performed using Imaris software (Bitplane). Every single cell expressing Oct4 in the embryonic compartment and every *T*/Brachyury-expressing cell was plotted on a projection of all cells in the structure. Cells

expressing *T/Brachyury* were represented as green dots and every other cell in the embryonic compartment was represented as a red dot.

Mitosis in mesoderm regions in ETX embryos and E6.75 embryos. Cells positive for H3S10-P protein expression were counted in the mesoderm region and outside this region. This procedure was repeated for three chosen *z* planes. *Z* planes were selected from the top (1/3 of total), middle (2/3 of the total) or end (3/3 of the total) region of each ETX embryo or natural embryo, and the values obtained were averaged. Student's *t*-test was performed.

Time-lapse imaging. Confocal time-lapse imaging during ETX embryo culture was performed using a spinning-disc microscope (3i), using a Zeiss EC Plan-NEOFLUAR ×20/0.5 objective. The embryos were imaged every 45 min in 100 µm image stacks of 4 µm *z* planes. Images were processed using Slidebook 5.0 (3i). Cell tracking time-lapse images were captured using an inverted SP8 confocal microscope (Leica Microsystems), using a Leica Fluotar VISIR 0.95 NA ×25 objective. Images were acquired in 6 min intervals with a *z* step of 1 µm. ETX embryos were imaged in a humidified chamber with 37 °C, 5% CO_2.

Whole mount in situ hybridization (WMISH). WMISH was performed exactly as previously described[32], with the only difference that the 10× DIG (digoxigenin)-blocking solution was prepared by dissolving 1 g of blocking reagent in 10 ml of malate buffer. Samples were digested with proteinase K for 3 min at room temperature with rocking. The probe for Cerl was provided by E. De Robertis, the probe for Nodal was provided by H. Hamada, the probes for Wnt3 and Bmp4 were provided by J. Rivera, and the probes for Cripto and T were provided by T. Rodriguez.

Cell isolation and qRT–PCR. After 5 or 6 days of culture, ETX embryos were collected. Asymmetric T expression was confirmed under a fluorescent microscope, and the TS compartment was dissected away. The ES compartment was cut through a line corresponding to the long axis, equivalent to the midline of an ETX embryo (perpendicular to the embryonic–extra-embryonic boundary). *T*:GFP-positive and negative domains were collected separately and transferred into lysis buffer (Life Technologies). Total RNA was extracted with the Arcturus Pico Pure RNA Isolation Kit, and qRT–PCR was performed with the Power SYBR Green RNA-to-CT 1-Step Kit (Life Technologies) and a Step One Plus Real-time PCR machine (Applied Biosystems). The amounts of mRNA were measured with SYBR Green PCR Master Mix (Ambion). Relative levels of transcript expression were assessed by the ΔΔCt method, with GADPH as endogenous control. For the qPCR primers used, see Supplementary Table 2.

Sample collection and RNA isolation. To collect RNA for RNA–seq, ETX embryos generated using a *T/Brachyury*-GFP reporter ES line were collected and TS compartments were dissected away. The ES compartment was further dissected in half on the long side and each half was analysed separately under a fluorescent microscope to identify GFP +ve (prospective posterior) and GFP −ve (prospective anterior) cells. Samples were collected in lysis buffer (2.3 µl of 0.2% Triton X-100 (Sigma) supplemented with 1 U μl^{-1} RNAsIN (Ambion)) and stored at −80 °C until library preparation.

Library preparation, RNA–seq and mapping of reads. Low-input RNA–seq was performed using the Smart-seq2 protocol[33,34], using 18 cycles of amplification in the PCR preamplification step. A pool of indexed libraries was sequenced on a HiSeq2500 in rapid run mode. Reads were mapped to the *Mus musculus* genome (Ensembl version 38.77) and quantified using the HTSeq-count[35].

Quality assessment and preprocessing of RNA–seq data. The quality of the reads was evaluated using the FASTQC tool[36]. The density distribution of gene expression for all samples was also plotted to assess sample consistency. Raw reads were mapped to the mm10 version of the mouse genome using the Tophat2 v2.0.4 program[37]. Samples with raw sequencing reads count of >10 million and mapping ratio of >50% were retained for further analysis. We calculated the fragment per kilobase per million (FPKM) as expression level using Cufflinks v2.0.2 with default parameters[38]. Genes with FPKM value >1.0 in at least one sample across all samples were retained for further analysis. Finally, the expression levels were transformed to logarithmic space by using $\log_2(FPKM + 1)$. With these criteria, three ETX embryos were retained for further analysis (ETX-A, ETX-B and ETX-C) and, because they were cut in half, each side was arbitrarily called side 1 or side 2.

Principal component analysis. PCA was based on all the expressed genes as described in the RNA–seq data preprocessing and was performed using the FactoMineR package in R.

Differentially expressed gene analysis. DEGs between ETX embryo side 1 and ETX embryo side 2 were identified using RankProd[39] with *P* value of <0.05 and fold change of >1.5. Heatmaps were generated using Cluster 3.0 and JavaTreeView[40].

Functional enrichment analysis. Functional enrichment of gene sets identified as differentially expressed between samples was performed using the Database for Annotation, Visualization and Integrated Discovery v6.8 (DAVID v6.8)[41].

Zip code mapping and corn plot analysis to compare side 1 and side 2 of ETX embryos to regions of the epiblast. Transcriptome data from each side of the ETX embryos were compared to embryo samples at three different stages (E6.5: 13 laser capture microdissection (LCM) samples; E7.0: 42 LCM samples; E7.5: 46 LCM samples). The reference embryo samples were subdivided into different epiblast regions as previously described[27]. To assess the similarity between ETX embryos and natural embryo samples, a Pearson correlation coefficient (PCC) was calculated as a measure of the correlation between the gene expression of reference embryo samples (E6.5: 13 samples; E7.0: 42 samples; E7.5: 46 samples) and transcriptome data from cells isolated from each side of the ETX embryos. A PCC of 1 indicated that the gene expression pattern of a sample taken from the ETX embryo and a region of the epiblast were identical, and therefore the two were perfectly correlated. Conversely, a PCC of 0 would indicate no correlation. Therefore, a high PCC value reflects closely matching gene expression patterns between the ETX embryo samples and post-implantation reference samples, whereas a low PCC reflects no match. This PCC was calculated based on the expression of 'zip code' genes identified as robust markers of different regions of the epiblast of the post-implantation embryo[27]. The PCC values for each side of the ETX embryo sample compared to each region of the epiblast for each reference embryo was depicted in the form of a 'corn plot' using MATLAB (version 2015a)[27].

Building the NJ tree. For combined ETX embryo and natural embryo samples, we first removed batch effects with ComBat (package in R) if individual samples were from different batches. Then, the Euclidean distance of any two samples was calculated based on DEGs, and then fed into MEGA (version: 7.0) software to build the NJ tree (under the Phylogeny menu).

Statistics and reproducibility. Statistical tests were performed on GraphPad Prism 7.0 software for Windows. Data were checked for normal distribution and equal variances before each parametric statistical test was performed. Qualitative data are presented as a contingency table and were analysed with Fisher's exact test. Where appropriate, Student's *t*-tests (two groups) or analysis of variance (multiple groups) were performed with Welch's correction if variance between groups was not equal. Error bars represent s.e.m. or s.d. as specified. Figure legends indicate the number of independent experiments performed in each analysis. Unless otherwise noted, each experiment was performed at least three times.

Data availability. RNA–seq data that support the findings of this study have been deposited in the Gene Expression Omnibus (GEO) under accession code GSE110105. LCM sequencing data are available under accession no. GSE65924.

Source data for RT–qPCR experiments (Fig. 4c and Supplementary Fig. 2i) and quantifications of the immunofluorescence data (Figs. 1f, 2a–c and 3e and Supplementary Figs. 2d-f-g, 4c and 5d,h) and the DEG list (Fig. 7b) are provided in Supplementary Table 3.

All other data supporting the findings of this study are available from the corresponding author on reasonable request.

References

28. Bedzhov, I., Leung, C. Y., Bialecka, M. & Zernicka-Goetz, M. In vitro culture of mouse blastocysts beyond the implantation stages. *Nat. Protoc.* **9**, 2732–2739 (2014).
29. Fehling, H. J. et al. Tracking mesoderm induction and its specification to the hemangioblast during embryonic stem cell differentiation. *Development* **130**, 4217–4227 (2003).
30. Rhee, J. M. et al. In vivo imaging and differential localization of lipid-modified GFP-variant fusions in embryonic stem cells and mice. *Genesis* **44**, 202–218 (2006).
31. Sozen, B., Amadei, G., Na, E., Michel, G. & Zernicka-Goetz, M. Stem cells reconstituting gastrulating embryo-like structures in vitro. *Nat. Protoc. Exch.* https://doi.org/10.1038/protex.2018.072 (2018).
32. Piette, D., Hendrickx, M., Willems, E., Kemp, C. R. & Leyns, L. An optimized procedure for whole-mount in situ hybridization on mouse embryos and embryoid bodies. *Nat. Protoc.* **3**, 1194–1201 (2008).
33. Picelli, S. et al. Smart-seq2 for sensitive full-length transcriptome profiling in single cells. *Nat. Methods* **10**, 1096–1098 (2013).
34. Picelli, S. et al. Full-length RNA-seq from single cells using Smart-seq2. *Nat. Protoc.* **9**, 171–181 (2014).
35. Anders, S., Pyl, P. T. & Huber, W. HTSeq—a Python framework to work with high-throughput sequencing data. *Bioinformatics* **31**, 166–169 (2015).
36. Andrews, S. *FastQC a Quality Control to Tool for High Throughput Sequence Data* https://www.bioinformatics.babraham.ac.uk/projects/fastqc/ (2010).
37. Trapnell, C., Pachter, L. & Salzberg, S. L. TopHat: discovering splice junctions with RNA–Seq. *Bioinformatics* **25**, 1105–1111 (2009).

38. Kim, D. et al. TopHat2: accurate alignment of transcriptomes in the presence of insertions, deletions and gene fusions. *Genome Biol.* **14**, R36 (2013).
39. Hong, F. et al. RankProd: a bioconductor package for detecting differentially expressed genes in meta-analysis. *Bioinformatics* **22**, 2825–2827 (2006).
40. Saldanha, A. J. Java Treeview—extensible visualization of microarray data. *Bioinformatics* **20**, 3246–3248 (2004).
41. Huang da, W., Sherman, B. T. & Lempicki, R. A. Systematic and integrative analysis of large gene lists using DAVID bioinformatics resources. *Nat. Protoc.* **4**, 44–57 (2009).

nature research

Corresponding author(s): Magdalena Zernicka-Goetz

Reporting Summary

Nature Research wishes to improve the reproducibility of the work that we publish. This form provides structure for consistency and transparency in reporting. For further information on Nature Research policies, see Authors & Referees and the Editorial Policy Checklist.

Statistical parameters

When statistical analyses are reported, confirm that the following items are present in the relevant location (e.g. figure legend, table legend, main text, or Methods section).

n/a	Confirmed	
☐	☒	The exact sample size (*n*) for each experimental group/condition, given as a discrete number and unit of measurement
☐	☒	An indication of whether measurements were taken from distinct samples or whether the same sample was measured repeatedly
☐	☒	The statistical test(s) used AND whether they are one- or two-sided *Only common tests should be described solely by name; describe more complex techniques in the Methods section.*
☐	☒	A description of all covariates tested
☐	☒	A description of any assumptions or corrections, such as tests of normality and adjustment for multiple comparisons
☐	☒	A full description of the statistics including central tendency (e.g. means) or other basic estimates (e.g. regression coefficient) AND variation (e.g. standard deviation) or associated estimates of uncertainty (e.g. confidence intervals)
☐	☒	For null hypothesis testing, the test statistic (e.g. *F*, *t*, *r*) with confidence intervals, effect sizes, degrees of freedom and *P* value noted *Give P values as exact values whenever suitable.*
☒	☐	For Bayesian analysis, information on the choice of priors and Markov chain Monte Carlo settings
☐	☒	For hierarchical and complex designs, identification of the appropriate level for tests and full reporting of outcomes
☐	☒	Estimates of effect sizes (e.g. Cohen's *d*, Pearson's *r*), indicating how they were calculated
☐	☒	Clearly defined error bars *State explicitly what error bars represent (e.g. SD, SE, CI)*

Our web collection on statistics for biologists may be useful.

Software and code

Policy information about availability of computer code

Data collection	The basic command used for data preparation. Tophat -p 16 -g 1 -N 2 --microexon- search --no-novel-juncs -G refGene.gtf -o out/ genome R1.fastq R2.fastq Cufflinks -p 16 -o out/ -g refGene.gtf accepted_hits.bam

Data analysis	- Immunofluorescence and time-lapse images: analyzed with Fiji (version 1.0) or Imaris (Bitplane). - Statistical analyses (excluding the deep-sequencing data): analyzed with GraphPad Prism (version 6) and Microsoft Excel - Analysis of deep-sequecing data, analysed with; R (version: 3.4.0) Python (version:2.7.13) Matlab (version: 2015a) Tophat (version: 2.0.4) Cufflinks (version: 2.0.4) DAVID (Database for Annotation, Visualisation and Integrated Discovery, version:6.8) MEGA (version:7.0) Cluster 3.0

For manuscripts utilizing custom algorithms or software that are central to the research but not yet described in published literature, software must be made available to editors/reviewers upon request. We strongly encourage code deposition in a community repository (e g. GitHub). See the Nature Research guidelines for submitting code & software for further information.

Data

Policy information about availability of data

All manuscripts must include a data availability statement. This statement should provide the following information, where applicable:

- Accession codes, unique identifiers, or web links for publicly available datasets
- A list of figures that have associated raw data
- A description of any restrictions on data availability

RNA–seq data that support the findings of this study have been deposited in the Gene Expression Omnibus (GEO) under accession code GSE110105. LCM sequencing data is available under accession number GSE65924. Source Data for RT–qPCR experiments (Fig. 4c, Supplementary Fig. 2i) and quantifications of the immunofluorescence data (Fig. 1f, Fig. 2a-b-c, Fig. 3e, Supplementary Fig. 2d-f-g, Supplementary Fig. 4c, Supplementary Fig. 5d, h) and the differentially expressed gene list (Fig. 7b) have been provided in Supplementary Table 3. All other data supporting the findings of this study are available from the corresponding author on reasonable request.

Field-specific reporting

Please select the best fit for your research. If you are not sure, read the appropriate sections before making your selection.

☒ Life sciences ☐ Behavioural & social sciences ☐ Ecological, evolutionary & environmental sciences

For a reference copy of the document with all sections, see nature.com/authors/policies/ReportingSummary-flat.pdf

Life sciences study design

All studies must disclose on these points even when the disclosure is negative.

Sample size	No statistical method was performed to predetermine sample size. Sample size for each experiment described in the paper based on our previous experience and the work of other groups using embryos and stem cells as experimental model systems.
Data exclusions	Culture experiments: on principle, data were only excluded for failed experiments, reasons for which included suboptimal culture conditions. ETX embryo samples for deep-sequencing analysis: those samples that did not pass the quality controls were excluded from the analysis The quality of the reads was evaluated using the FASTQC tool. Density distribution of gene expression for all samples was also plotted to assess sample consistency. Raw reads were mapped to mm10 version of the mouse genome using the Tophat2 v2.0.4 program. Samples with raw sequencing reads count > 10 million and mapping ratio > 50% were retained for further analysis. We calculated fragment per kilobase per million (FPKM) as expression level using Cufflinks v2.0.2 with default parameters. Genes with the FPKM value > 1.0 in at least one sample across all samples were retained for further analysis. Finally, the expression levels were transformed to logarithmic space by using log2 (FPKM +1). With these criteria, 3 gastrulating ETX embryos were retained for further analysis (GE-A, GE-B and GE-C) and since they were cut in half, each side was arbitrarily called side 1 or side 2.
Replication	In the study, all attempts at replication were successful. Each result described in the paper is based on at least two independent biological replicates but very often an experiment is based on more

than two experiments. Figure legends indicate the number of independent experiments performed in each analysis.

Randomization

For experiments were our samples were exposed to chemical inhibitors, samples were randomly allocated to control and experimental groups.

Blinding

Investigators were not blinded.
This study compares ETX embryos to natural embryos. The experiments were descriptive in nature.

Reporting for specific materials, systems and methods

Materials & experimental systems

n/a	Involved in the study
☒	☐ Unique biological materials
☐	☒ Antibodies
☐	☒ Eukaryotic cell lines
☒	☐ Palaeontology
☐	☒ Animals and other organisms
☒	☐ Human research participants

Methods

n/a	Involved in the study
☒	☐ ChIP-seq
☒	☐ Flow cytometry
☒	☐ MRI-based neuroimaging

Antibodies

Antibodies used

The following antibodies were used:
Oct 3/4 (mouse), C-10, Santa cruz sc-5279 1:200, Lot:E1017
Tbr2/Eomes (rabbit) abcam ab23345 1:400 Lot:GR305614-2
Brachyury/T (goat) Santa cruz sc-17745, C-19, 1:500 (discontinued)
Brachyury/T (goat) R&D systems AF2085 1:500, Lot:KQP0617031
Podocalyxin (rat) Clone 192703 R&D systems MAB1556 1:400, Lot:IPF0317051
GFP (rat) Clone GF090R Nacalai biochemicals 04404-84 ,1:2000, Lot:M8E4658
Tfap2c (rabbit) Santa cruz, H-77, sc-8977, 1:200 (discontinued)
Laminin (rabbit) Sigma L9393 1:400, Lot:046M4837V
Collagen IV (rabbit), abcam ab19808, 1:200, Lot:GR261208-14
E-cadherin (rat) Clone ECCD-2 Life Technologies (Thermofisher scientific) 13-1900, 1:400, Lot:74960345A
N-cadherin (mouse) BD Biosciences, 610920, 1:400, Lot:7124538
GM130 (mouse) Clone 35/GM130 BD Biosciences 610822 1:500
Anti-phospho-Histone H3 (Ser10), Millipore, 06-570, 1/500, Lot:29480
Gata6 (Goat) R&D Systems, AF1700, 1:200, Lot:KWT0316081
Gata4 (Goat) Santa cruz sc-1237, C20, 1:200, Lot:J2015
Foxa2 (Rabbit) Cell signalling technologies, D56D6, 8186 1:200, Lot:3
Sox17 R&D Systems, AF1924, 1:200, Lot:KGA091621
Otx2 (Goat) R&D Systems, AF1979, 1:200, Lot:KNO0615111 and Lot:KNO0616081
Lefty1 (goat) R&D Systems, AF746, 1:2000, Lot: CMM021805A
F-actin (Phalloidin 488) Life Technologies (Thermofisher scientific), A12379, 1:1000, Lot:1896875
Alexa 488 (Donkey anti-rat) Life Technologies (Thermofisher scientific), A21208, 1:500, Lot:1900239
Alexa 568 (Donkey anti-mouse) Life Technologies (Thermofisher scientific), A10037, 1:500, Lot:1917938
Alexa 647 (Donkey anti-rabbit) Life Technologies (Thermofisher scientific), A31573, 1:500, Lot:190516
Alexa 647 (Donkey anti-goat) Life Technologies (Thermofisher scientific), A21447, 1:500, Lot:1917928

This information is also included in Supplementary Table 1.

Validation

The subcellular localization of all the proteins analyzed in this study has been previously reported in mouse embryo/stem cell studies (shown as immunoflourescence labelling).

Oct4: it specifically stained the epiblast at all stages tested, as expected (Science 356, doi:10.1126/science.aal1810).
Eomes: it correctly stained Exe and embryonic VE as reported and as expected (Science 356, doi:10.1126/science.aal1810).
Bry: it correctly stained mesoderm at 6.5 and later as reported and expected (Dev Biol 288, 363-371).
Podocalyxin: correclty stained polarized lumen in the embryo as reported elsewhere (Nature 552, 239-243).
Tfap2c: it correctly stained the ExE lineage in postimplantation embryos and PGC after gastrulation as reported and expected (Science 356, doi:10.1126/science.aal1810).
Laminin: it correctly stained the basement membrane between visceral endoderm and Exe or epiblast, as reported elsewhere and as expected (Dev Dyn 241, 270-283)

Collagen: same as above (Dev Dyn 241, 270-283)
E-cadherin: it correctly stained the basolateral side of cells in the embryo as reported and as expected (Science 356, doi:10.1126/science.aal1810)
Ncadherin: it correctly displayed upregulation on the side of the epiblast undergoing epithelial to mesenchymal transition as reported and as expected (eLife 2018;7:e32839)
Gm130: it correctly displayed the punctate Golgi morphology (Nature 552, 239-243).
Anti phospho histone 3 it correctly labelled mitotic cells, as expected (Science, 360(6384):99-102 2018)
Gata6: it correctly labelled the visceral endoderm in postimplantation embryos (eLife 2018;7:e32839)
Gata4: same as above (Science 356, doi:10.1126/science.aal1810)
Foxa2: it was correctly expressed in the visceral endoderm and in the gastrulation stage mesoderm (Development 136, 1029-1038)
Sox17: it was correctly expressed in the visceral endoderm (eLife 2018;7:e32839)
Otx2: it was correctly expressed in the epiblast and embryonic visceral endoderm of post-implantation embryos (eLife 2018;7:e32839)
Lefty1: it was correctly expressed specifically on the anterior side of the embryonic visceral endoderm of developing postimplantation embryos starting at E5.5 and beyond (Dev. Biol. 402 (2015) 175-191).
F-actin: it correctly stained the cell membrane and was apically enriched, as expected and reported it correctly stain (Development, 138(2011) 3011-3020).

Eukaryotic cell lines

Policy information about cell lines

Cell line source(s)	The following cell lines were used: Mouse embryonic stem cells: E14 WT mESCs (kindly provided by Prof. Austin Smith, Stem Cell Institute, Cambridge, UK), Nodal HBE-YFP ESCs and T:GFP ESCs kindly provided by Dr. Alfonso Martinez Arias, Cambridge, UK) Mouse trophoblast stem cells: wild-type TSCs (a gift from Jenny Nichols, University of Cambridge, UK) Mouse extraembryonic endoderm cells: wild-type XENs (a gift from Ellen Na, University of Charité, Germany) and EGFP XENs (a gift from Dr. Peter Rugg-Gunn Babraham Institute, Cambridge).
Authentication	Cells were maintained in conditions to preserve stem cell character and prevent differentiation. Plates were inspected for morphological evidence of differentiation (altered colony morphology in ESC cultures or presence of trophoblast giant cells in TSC cultures..etc) and plates with differentiated cells were discarded. Furthermore, cell identities were confirmed routinely by immunoflourescence marker expressions.
Mycoplasma contamination	Cell lines were routinely tested for mycoplasma contamination by PCR and confirmed that they were negative for mycoplasma contamination.
Commonly misidentified lines (See ICLAC register)	The cells we used are not part of this database

Animals and other organisms

Policy information about studies involving animals; ARRIVE guidelines recommended for reporting animal research

Laboratory animals	6-week old mice (Mus musculus) were used to obtain mouse embryos for this study. The following strains and genetically-modified models were used: F1 (C57Bl6xCBA), MF1, CD1, and T:GFP (both males and females).
Wild animals	no wild animals were used in the study.
Field-collected samples	no field-collected samples were used in the study.